

Transport in a coordinated soil-root-xylem-phloem leaf system

Cheng-Wei Huang ^{a,*}, Jean-Christophe Domec ^{b,c}, Sari Palmroth ^b, William T. Pockman ^a, Marcy E. Litvak ^a, Gabriel G. Katul ^{b,d,e}

^a Biology Department, University of New Mexico, Albuquerque, NM, USA

^b Nicholas School of the Environment, Duke University, Durham, NC, USA

^c UMR INRA-ISPA 1391, Bordeaux Sciences Agro, Gradignan 33195, France

^d Department of Civil and Environmental Engineering, Duke University, Durham, NC, USA

^e Karlsruhe Institute of Technology (KIT), Institute of Meteorology and Climate Research, Kreuzeckbahnstrae 19, Garmisch-Partenkirchen 82467, Germany

ARTICLE INFO

Keywords:

Acclimation

Isohydric-to-anisohydric behavior

Marginal water use efficiency

Phloem

Stomatal response

Xylem

ABSTRACT

Links between the carbon and water economies of plants are coupled by combining the biochemical demand for atmospheric CO₂ with gas transfer through stomates, liquid water transport in the soil-xylem hydraulic system and sucrose export in the phloem. We formulated a model to predict stomatal conductance (g_s), consistent with the maximum energy circulation concept of Lotka and Odum, by maximizing the sucrose flux out of photosynthesizing leaves. The proposed modeling approach recovers all prior results derived from stomatal optimization theories and profit-maximization arguments for the xylem hydraulic system aimed at predicting g_s . The novel features of this approach are its ability to 1) predict the price of losing water in carbon units using xylem and phloem properties (i.e., the marginal water use efficiency) and 2) explain why water molecules become more expensive to exchange for CO₂ molecules when soil moisture becomes limiting or when plants acclimate to new elevated atmospheric CO₂ concentration. On short time-scales (sub-daily), predicted g_s under many environmental stimuli were consistent with measurements reported in the literature, including a general sensitivity of g_s to vapor pressure deficit and leaf water potential. During progressive droughts, differences in the coordination among the leaf, xylem, and phloem functioning determine the isohydric-to-anisohydric behavior among plants.

1. Introduction

Stomata evolved more than 400 million years to regulate gas exchange with a desiccating atmosphere, allowing land plants to spread across the earth's surface. Environmental responses of stomata are now prominently featured as a research priority in many studies on climate change, food security, and food-energy-water nexus (Betts et al., 2007; Cox et al., 2000; Gedney et al., 2006; Hetherington and Woodward, 2003). As plants adapted to a terrestrial environment, they competed for light and utilized increasing height to enhance their capacity to photosynthesize. Height facilitates a productive display of photosynthetic machinery by allowing a vertical distribution of chlorophyll so that light-use efficiency can be increased relative to a concentrated display of chlorophyll (Gratani, 2014). Increased height further required selection for solutions to improve water delivery to leaves and carbohydrate translocation from leaves to reserves, root exudation, and export to symbionts (Fatichi et al., 2014; Pittermann, 2010; Thompson and Katul, 2012).

It is now accepted that a framework linking stomatal function to such water delivery and trans-location of carbohydrates is needed to assess

how vegetation structure and its spatial patterns is impacted by future climate conditions, and vice versa (Hölttä et al., 2017; Jensen et al., 2016; Mencuccini and Hölttä, 2010; Nikinmaa et al., 2013; Savage et al., 2015; Sevanto, 2014; Sperry and Love, 2015). The general features of this framework rely upon the cohesion-tension (CT) theory of sap ascent in the xylem (Dixon and Joly, 1895), osmosis and pressure-driven transport in the phloem through the Münch mechanism (Jensen et al., 2016), and stomatal optimization theories (SOT) in leaves linking the carbon and water economies of plants (Cowan and Farquhar, 1977). The latter approach, while lacking the physical basis of the other two, has been reasonably successful in explaining short-term responses of leaf gas-exchange to variations in photosynthetically active radiation (PPFD), air temperature (T_a), atmospheric CO₂ concentration (c_a), and atmospheric aridity (Buckley et al., 2016; Damour et al., 2010; Katul et al., 2012; 2009; Medlyn et al., 2011; Paschalis et al., 2017). Because stomatal function balances photosynthetic carbon gain and water loss (transpiration) to the atmosphere, a number of arguments have been offered to displace the original SOT at the leaf scale (Cowan and Farquhar, 1977). At the whole-plant level, soil-xylem hydraulics (i.e., outcome of supply and demand for water) and carbohydrate (mainly

* Corresponding author.

E-mail addresses: ch224@unm.edu (C.-W. Huang), jc.domec@duke.edu (J.-C. Domec), sari.palmroth@duke.edu (S. Palmroth), pockman@unm.edu (W.T. Pockman), mlitvak@unm.edu (M.E. Litvak), gaby@duke.edu (G.G. Katul).

sucrose) transport efficiency in the phloem impose appreciable constraints so as to govern leaf-level gas exchange (Hölttä et al., 2017; 2006; Jensen et al., 2016; Mencuccini and Hölttä, 2010; Nikinmaa et al., 2013; Savage et al., 2015; Sevanto, 2014; Sperry and Love, 2015).

The work here shows that the original SOT at the leaf scale (Cowan and Farquhar, 1977), the maximization of water flow in the xylem (and variants on them), the maximization of carbohydrate transport, and attainment of a near-constant inter-cellular to ambient atmospheric CO₂ hypothesis (Prentice et al., 2014) all lead to similar formulations for stomatal conductance under well-watered soil condition. What is different across these approaches is the interpretation of parameters (e.g., the cost term used to maximize or minimize the objective function) and their short-term responses to boundary conditions such as root-zone soil moisture and changes in c_a . Despite differences in what these approaches maximize (or minimize), a similarity in outcome may be hinting that a more general principle is governing plant responses to fluctuating environmental conditions, the main focus of the work here.

Our conjecture is that plants may have evolved a coordinated photosynthetic-hydraulic-sucrose transporting machinery that confers some competitive advantages in fluctuating environmental conditions. Such a coordination should manifest itself in linkages between the properties describing the photosynthetic machinery, the hydraulic and carbohydrate transporting systems. It will be remiss if analogies to the energetics of evolution principle as a consequence of natural selection, proposed in 1922 by Lotka (Lotka, 1922; Odum and Hall, 1995), are not pointed out. This principle states that “Natural selection tends to make the energy flux through the system a maximum, so far as compatible with the constraints to which the system is subject.” As indicated by Lotka, the maximum input of energy flux exceeding the actual energy demand (for growth, maintenance, defense and reproduction) at the current states offers a great opportunity in the future to develop an advantageous plant body that can promote larger total energy flux through the system. In the plant kingdom, the input of energy flux can be expressed as the sucrose flux rendered out of the loading leaf. Environmental conditions and endogenous transport processes affecting this energy flux represent the limiting constraints to the system. It is with this view that coordination among the xylem, phloem, and leaf is interpreted as an energy-capturing device to direct available energy into the system by harvesting limited resources (Lotka, 1922).

1.1. Hypothesis

In light of the energetics of the evolution principle (Lotka, 1922), we hypothesize that stomatal conductance (g_s) can be predicted by assuming coordination in the leaf-xylem-phloem system thereby recovering the mathematical form of the aforementioned approaches. The criterion for predicting g_s is that this coordination maintains efficient (maximum) transport rate of photoassimilates (i.e., energy flux) out of the loading zone over short time intervals (Δt) so as to ensure maximum energy circulation at the whole-plant level. When coupling the transport and physiological processes in the leaf-xylem-phloem system (i.e., photosynthetic machinery, water transport in xylem and export of assimilated sugar from loading phloem), how the limiting constraints induced by these processes and their interaction impact the energy flux entering the plant system and subsequently g_s are now considered explicitly in this new modeling approach. Specifically, this hypothesis offers a number of advantages: (1) the phloem transport efficiency is no longer isolated from the photosynthetic machinery, soil-xylem hydraulics and stomatal function as is now recognized (Hölttä et al., 2017; Jensen et al., 2016; Mencuccini and Hölttä, 2010; Nikinmaa et al., 2013; Sevanto et al., 2014); (2) the hypothetical assumption of pricing water loss in SOT or fitness costs of low xylem water potential in profit-maximization is by-

passed. It should be noted that the transport rate of photoassimilates out of the loading zone represents the objective function to be maximized, which is similar to the non-steady state model proposed elsewhere (Nikinmaa et al., 2013). Adopting this hypothesis, the objective of this work is to analyze g_s responses to environmental factors and plant attributes across a wide range of time-scales. We also focus specifically on two consequences of the model results: (i) The g_s responses to long-term elevated-CO₂ conditions and (ii) progressive drought as well as species differentiation across the spectrum of isohydric-to-anisohydric behavior. Before presenting the model formulation, the constraints on photosynthesis and xylem-water movement are briefly reviewed with a lens on their connections.

1.2. Constraints on photosynthesis and water transport

For C3 plants, the photosynthetic machinery limits the biochemical demand for CO₂ ($f_{c,d}$). Mathematically, $f_{c,d}$ can be expressed as the outcome of co-limitation of Ribulose-1,5-bisphosphate carboxylase/oxygenase (Rubisco) kinetic activity and Ribulose-1,5-biphosphate (RuBP) regeneration rate (Farquhar et al., 1980b) approximated by Vico et al. (2013):

$$f_{c,d} = \frac{k_1(c_i - \Gamma^*)}{k_2 + c_i} - R_d, \quad (1)$$

where c_i is the inter-cellular CO₂ concentration, k_1 and k_2 are photosynthetic parameters that vary with PPFD and T_a , Γ^* is the CO₂ compensation point in the absence of mitochondrial respiration, and R_d is the daytime mitochondrial respiration rate. Eq. (1) is a hyperbolic function imposing the most limiting factor through electron transport rate at high c_i (i.e., $f_{c,d} \approx J/4 - R_d$ when $k_1 = J/4$ where J is the electron transport rate) or through Rubisco activity at low c_i (i.e., $f_{c,d} \approx V_{c,max}(c_i - \Gamma^*)(c_i + a_2) - R_d$ when $k_2 = k_1 a_2 / V_{c,max}$ where $V_{c,max}$ is the maximum carboxylation capacity and $a_2 = K_c(1 + C_{oa}/K_o)$ where C_{oa} is the oxygen concentration in the atmosphere and K_c and K_o are respectively the Michaelis constants for CO₂ fixation and oxygen inhibition) (Vico et al., 2013). When operating under co-limitation regime, Eq. (1) also ensures a continuous transition between the two photosynthetic limitations. For $c_i \rightarrow \infty$, $f_{c,d}$ saturates at a maximum $f_{c,max} = k_1 - R_d$ (i.e., the asymptotic behavior of $f_c - c_i$ curve; $f_{c,d}|_{c_i \rightarrow \infty} = k_1(c_i - \Gamma^*)/(k_2 + c_i) - R_d|_{c_i \rightarrow \infty}$). Hence, when c_i availability is not limiting, photosynthesis is only constrained by the photosynthetic machinery usually through electron transport (RuBP limitation; L1 in Fig. 1). Although an infinite c_i is not realistic for any condition, this extreme case may be used to explain the rapid land colonization by plants in the Ordovician and their subsequent productivity during the Silurian-Devonian approximately 400 million years ago. During this time period, c_a reached up to 5000 ppm (Berner, 1991; Berner and Kothavala, 2001) and the long-term c_i/c_a commonly ranged from 0.6 to 0.9 (Drake et al., 1997; Ehleringer and Cerling, 1995; Prentice et al., 2014; Wong et al., 1979). It was this era when photorespiration was potentially suppressed and water use efficiency remained high (Sperry, 2003).

For present c_a conditions (≈ 400 ppm), the assimilation rate is further limited by the atmospheric supply of CO₂, which in turn is governed by c_a , the transport efficiency to CO₂ through the stomatal pathway (i.e., stomatal conductance; g_s), and the laminar boundary layer attached to the leaf surface. Assuming an infinitesimal thickness of the laminar boundary layer (i.e., well-coupled condition) and a mesophyll conductance to CO₂ that is much larger than g_s , the atmospheric supply of CO₂ across the stomatal aperture can be described by a Fickian diffusion and is given as $f_{c,s} = g_s(c_a - c_i)$. If all CO₂ molecules diffusing through stomata are eventually assimilated, then the supply and demand for CO₂ are in balance resulting in $f_{c,s} = f_{c,d}$. The $f_{c,s} = f_{c,d}$ results in an actual photosynthetic rate (f_c) that can then be expressed as a function of g_s and the photosynthetic parameters (Huang et al., 2015; Katul et al., 2010):

$$f_c(g_s) = \frac{1}{2}[k_1 + (k_2 + c_a)g_s - R_d]$$

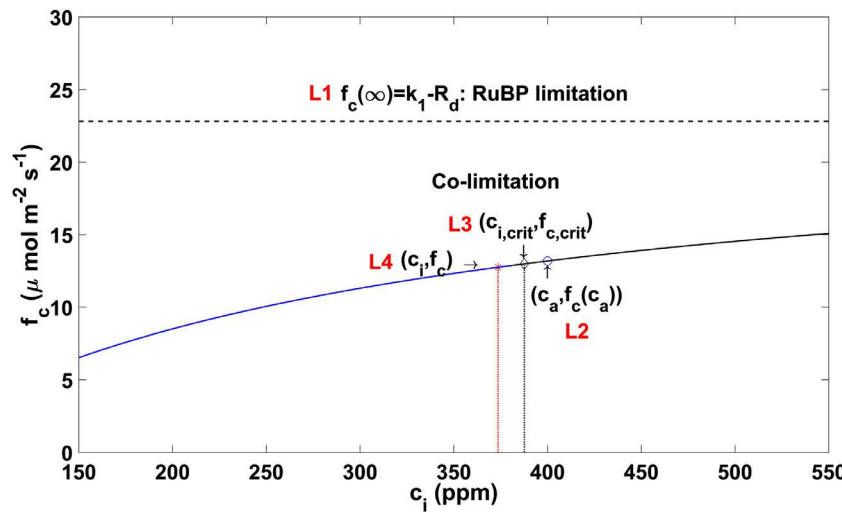


Fig. 1. The biochemical demand ($f_c - c_i$) curve featuring the various mechanisms (L1-L4) limiting photosynthesis (L1: limitation of the photosynthetic machinery when $c_i \rightarrow \infty$, L2: limitation of atmospheric CO_2 concentration when $c_i \rightarrow c_a$, L3: soil-xylem hydraulic limitation representing the maximum permissible $f_{c, crit}(c_{i, crit})$ at critical $\psi_{i, crit}$, L4: limitation of a coordinated photosynthetic-hydraulic-sucrose transporting machinery). How these limitations (i.e., L1-L4) impact f_c that can operate along the $f_c - c_i$ curve is presented. The physiological, hydraulic and allometric attributes of soil-plant system for coniferous species in general reported elsewhere (Huang et al., 2017) are adopted. The $K - \psi_i$ is reconstructed using a multi-layer plant hydraulic model described elsewhere (Huang et al., 2017; Sperry et al., 1998). Physical characteristics of leaves and anatomical attributes of phloem for *Pinus taeda* L. listed in Table 2 are used. The sugar loading efficiency (α) is assumed to be 1 (Hölttä et al., 2017; Nikinmaa et al., 2013). The result here is computed for well-watered soil condition when photosynthetically active radiation (PPFD), air temperature (T_a), atmospheric CO_2 concentration (c_a) and relative humidity (RH) are $1000 \mu\text{mol m}^{-2} \text{s}^{-1}$, 25°C , 400 ppm and 90% , respectively.

$$-\sqrt{[k_1 + (k_2 - c_a)g_s - R_d]^2 - 4g_s(-c_a g_s k_2 - k_2 R_d - k_1 \Gamma^*)}. \quad (2)$$

For $g_s \rightarrow \infty$ (i.e., stomata do not limit photosynthesis), $c_i \rightarrow c_a$ and a finite maximum $f_c = k_1(c_a - \Gamma^*)/(k_2 + c_a) - R_d$ is guaranteed (see Eq. (1)). Again, this is another reference condition where f_c is now bounded by finite c_a (L2 in Fig. 1). When $c_a \rightarrow \infty$, $f_{c, max}$ is recovered. For a finite g_s , f_c is limited by g_s (see Eq. (2)) as well as environmental conditions through their effects on k_1 , k_2 , and Γ^* . As shown later, such limitations are dictated by the coordinated photosynthetic-hydraulic-sucrose transporting machinery. Eq. (2) demonstrates that an additional and independent link between f_c and g_s is needed to mathematically solve for g_s , f_c , and c_i from $(c_i/c_a) = 1 - f_{c,s}/(g_s c_a)$. In current climate and land-surface models, this independent expression is provided using one of two semi-empirical formulations proposed by Ball et al. (1987) (BWB) and Leuning (1995) (LEU) thereby allowing f_c , g_s , and c_i to be predicted (Baldocchi and Meyers, 1998; Juang et al., 2008; Lai et al., 2000; Sellers et al., 1996; 1995; Siqueira and Katul, 2002). The common feature of BWB and LEU models is that $g_s = m_E(f_c/(c_a - \Gamma^*))F$ where m_E is an empirical parameter linking g_s to $f_c/(c_a - \Gamma^*)$ and the reduction function $F = RH$ or $(1 + D/D_0)^{-1}$ is an atmospheric aridity function where RH is the relative humidity, D is the vapor pressure deficit, and D_0 is a normalizing constant. How g_s is impacted by the measures of atmospheric aridity such as RH and D is included in BWB and LEU models. The linkage between g_s and f_c/c_a through F is perhaps not surprising when water loss through the stomatal pathway (i.e., atmospheric evaporative demand; $f_{e,d} \approx a g_s D/P_a$ where $a \approx 1.6$ is the relative diffusivity of water vapor with respect to CO_2 and P_a is the atmospheric pressure) is inevitable during photosynthesis. The g_s should satisfy both the atmospheric evaporative demand (i.e., $f_{e,d}$) and the supply-demand balance of CO_2 (i.e., $f_{c,s} = f_{c,d}$; Eq. (2)).

Such atmospheric evaporative loss from the leaf as driven by the biochemical demand for CO_2 and the aridity of the atmosphere only serves as an upper bound for water vapor loss. The actual water supply to satisfy the atmospheric evaporative demand also depends on soil water availability and whole-system hydraulic conductance (K) integrated throughout the entire water flow path commencing from the soil and progressing to the distal parts of the plants (Sperry and Love, 2015). When xylem water potential decreases, originally functional (i.e., water-

filled) xylem conduits can be occupied by air drawn from neighboring air-filled conduits through inter-conduit pit membranes such that water is no longer conducted by these dysfunctional conduits (Crombie et al., 1985; Sperry and Tyree, 1988; 1990). Similar to xylem, soil water conductivity that varies with decreasing water potential is also reduced by spreading air over pore space between soil particles. The BWB and LEU models do not explicitly or mechanistically consider how g_s is impacted by reductions in K due to progressive soil drying (i.e., soil-xylem hydraulic limitation). The effects of such soil drying is represented by ad-hoc reductions in m_E (Tuzet et al., 2003).

Based on the economics of leaf-level gas exchange (Berninger and Hari, 1993; Cowan and Farquhar, 1977; Givnish and Vermeij, 1976; Hari et al., 1986; Konrad et al., 2008), stomatal optimization theories (SOT) provide an alternative approach to predict g_s . In SOT, the stomatal aperture variation is assumed to maximize carbon gain subjected to a 'cost' of water loss incurred during transpiration in carbon units (cost function). This constrained optimization theory is equivalent to maximizing the objective function (or Hamiltonian) defined as:

$$H_{a,L}(g_s) = \underbrace{f_c(g_s)}_{\text{Gain}} - \underbrace{\lambda_L f_{e,d}(g_s)}_{\text{Cost}}, \quad (3)$$

$$\frac{\partial H_{a,L}(g_s)}{\partial g_s} = \frac{\partial f_c(g_s)}{\partial g_s} - \lambda_L \frac{\partial f_{e,d}(g_s)}{\partial g_s} = 0,$$

with $(\partial f_c/\partial g_s)/(\partial f_{e,d}/\partial g_s) = \lambda_L > 0$, where the cost function is determined by the unit cost of water loss, λ_L , also known as the marginal water use efficiency (or Lagrange multiplier). Under some conditions, the analytical form of g_s derived from SOT is *per se* similar to BWB and LEU models (Katul et al., 2010; 2012; Medlyn et al., 2011; Volpe et al., 2011). For the optimal solution to hold, λ_L must be a constant independent of short-term stomatal aperture fluctuations (e.g., sub-hourly) (Katul et al., 2009). However, λ_L may vary on longer time-scales such as those commensurate with drying soil (daily), or any structural acclimation or adaptation (monthly or yearly) (Buckley et al., 2016; Manzoni et al., 2013b). Stated differently, λ_L can be inferred from $(\partial f_c/\partial g_s)/(\partial f_{e,d}/\partial g_s)$ provided a large time-scale separation exists between the g_s - and λ_L -variability (Katul et al., 2010; Manzoni et al., 2011). Similar to BWB and LEU models, the representation of water loss in SOT ($f_{e,d}$) does not

directly account for water supply limitations imposed by the soil-xylem hydraulic system (Wolf et al., 2016). To capture such effects in drying soil conditions, an ad-hoc increase in λ_L with decreasing soil water status must be *a priori* specified (Manzoni et al., 2011). Soil-xylem hydraulics may offer a logical alternative to such ad-hoc specification.

A linkage between g_s and soil-xylem hydraulics can be obtained by the supply-demand balance for water (Manzoni et al., 2014; Sperry and Love, 2015; Sperry et al., 2016b) given as:

$$f_{e,s} = \frac{K(\psi_l)[\psi_s - \psi_l]}{m_v A_l} = \frac{a g_s D}{P_a} = f_{e,d}, \quad (4)$$

resulting in $g_s(\psi_l) = \frac{K(\psi_l)[\psi_s - \psi_l] P_a}{a D m_v A_l}$,

where $f_{e,s}$ represents the steady-state water supply function determined by the overall $K(\psi_l)$ and the total water potential difference between the soil (ψ_s) and the leaf xylem (ψ_l), m_v is the molecular weight of water, and A_l is the leaf area. When coupling the supply-demand balance of CO_2 (Eq. (2)) and water (Eq. (4)) fluxes through g_s , an $f_c(\psi_l)$ relation can be derived without invoking a cost function and its associated unknown parameter, λ_L , as in SOT. However, ψ_l is now necessary to determine f_c prompting interest in possible links between SOT and soil-xylem hydraulics.

As a necessary step to link soil-xylem hydraulics to SOT, two remarks are in order: (1) g_s is entirely described by ψ_l at a given ψ_s as given by Eq. (4) provided that the $K(\psi_l)$ is known, and (2) $f_c(g_s)$ is a monotonically increasing function with increasing g_s as dictated by Eq. (2). These two remarks imply that $f_c(g_s)$ is a maximum at the maximum g_s allowed by Eq. (4) and this maximum can be evaluated from $\partial g_s / \partial \psi_l = 0$. The associated leaf pressure satisfying $\partial g_s / \partial \psi_l = 0$ is hereafter referred to as $\psi_{l,crit}$. The water and CO_2 fluxes at $\psi_{l,crit}$ must represent the maximum permissible water transport capacity ($f_{e,crit}$) and the maximum permissible assimilation rate ($f_{c,crit}$) that can be supported by the soil-xylem hydraulic system to the leaf at a given ψ_s (Manzoni et al., 2013a; Sperry et al., 2002). To solve the equation $\partial g_s / \partial \psi_l = 0$ and determine $\psi_{l,crit}$, $K(\psi_l)$ must be *a priori* determined. There are multiple approaches to determine $K(\psi_l)$ at the plant scale that often necessitate detailed hydraulic models through the soil-root-xylem system (Bohrer et al., 2005; Huang et al., 2017; Manoli et al., 2014; Sperry et al., 1998). Notwithstanding this complication, $K(\psi_l)$ can be determined independently without requiring any knowledge of the photosynthetic properties or atmospheric drivers for g_s . Hence, unless otherwise stated, it is assumed that $K(\psi_l)$ is known and represents the up-scaled xylem hydraulic system. The supply-demand balance of water flux sets another physical limit on g_s because of $f_{e,crit}$ and thus f_c (L3 in Fig. 1). Last, it is to be noted that maximizing $f_c(\psi_l)$ is equivalent to maximizing $f_e(\psi_l)$. This further suggests that the consideration of supply-demand balance of CO_2 (Eq. (2)) and water (Eq. (4)) fluxes alone is not sufficient to predict the operating g_s and f_c (i.e., operating f_c is smaller than $f_{c,crit}$; L4 in Fig. 1). Moreover, the operating leaf pressure must be larger than $\psi_{l,crit}$ (or smaller in magnitude). To be shown later, the limitations in the co-ordinated photosynthetic-hydraulic-sucrose transporting system are required to determine the optimal operating leaf pressure for a given soil pressure.

A number of variants to this approach have also been proposed. For example, a modified SOT that accounts for the soil-xylem hydraulics can be expressed as (Novick et al., 2016):

$$\underbrace{H_{a,X}(\psi_l)}_{\text{Profit}} = \underbrace{f_c(\psi_l)}_{\text{Gain}} - \underbrace{\lambda_X f_e(\psi_l)}_{\text{Cost}} \quad (5)$$

$$\frac{\partial H_{a,X}(\psi_l)}{\partial \psi_l} = \frac{\partial f_c(\psi_l)}{\partial \psi_l} - \lambda_X \frac{\partial f_e(\psi_l)}{\partial \psi_l} = 0.$$

Because g_s is entirely described by ψ_l , Eq. (5) can be directly derived from Eq. (3) by noting that $\partial H_{a,X} / \partial g_s = (\partial H_{a,X} / \partial \psi_l)(\partial \psi_l / \partial g_s) = 0$ is equivalent to $(\partial H_{a,X} / \partial \psi_l) = 0$ when $|\partial \psi_l / \partial g_s|$ is always larger than zero (see Eq. (4)). The cost function in Eq. (5) represents the sought-after limitation on g_s and further includes soil-xylem hydraulics. As the modified

SOT explicitly accounts for the soil-xylem hydraulics at the whole-plant level to accommodate the effects of dry soil process (i.e., varying ψ_s and ψ_l) on g_s , Eq. (5) may be robust as λ_X is expected to be less variable when compared with its leaf-level λ_L counterpart in the conventional SOT. A pre-specified increasing function of λ_L with decreasing ψ_s is still required as discussed before. However, the specification of λ_X remains arbitrary. Another approach that bypasses the need for specifying λ_X altogether is to revise the objective function. A metric of marginal xylem tension efficiency (Wolf et al., 2016) or relative K losses (Sperry et al., 2016a) were recently suggested as alternatives to SOT (and are labeled as profit-maximization). Their mathematical form can be still framed explicitly as *Gain-Cost* thereby resembling $H_{a,X}$ but without the need for a λ_X . Next, sucrose production (by-product of photosynthesis) and their transport in the phloem may offer new constraints on the leaf-xylem hydraulic system (or the marginal water use efficiency) thereby mathematically closing the original problem linking xylem-leaf-phloem discussed in Section 1.

2. Theory

2.1. Modeling framework

The leaf-level gas exchange of water vapor and CO_2 , liquid water, and carbohydrate (assumed to be sucrose) mass fluxes in xylem and phloem are presented in Fig. 2 (a). The notations and units used throughout are listed in Table 1. As noted earlier, the relation between K and ψ_l here (see Eq. (4)) is reconstructed using a multi-layer plant hydraulic model described elsewhere (Huang et al., 2017; Sperry et al., 1998) and is not repeated. The basic elements of this hydraulic model are as follows: Hydraulic architecture for both above- and below-ground compartments are not explicitly resolved but indirectly accounted for in the whole-system hydraulic conductance (i.e., $K(\psi_l)$). The effects of plant water storage and hysteresis in $K - \psi_l$ relation induced by the delay in repair of cavitating xylem conduits (i.e., refilling) are also not considered here (see Section 3.4) but can be accommodated in the present framework. A number of features are pointed out regarding the numerical solution of the hydraulic model (i.e., $K - \psi_l$ relation): 1) the leaf water potential ψ_{12} at which hydraulic conductivity drops by 12% from its maximum value K_{max} can be determined from the derived $K - \psi_l$ relation and roughly coincides with the air-entry pressure (Domec and Gartner, 2001), and 2) ψ_{50} at which hydraulic conductivity drops by about 50%, which is often used in safety-efficiency studies, is never attained in practice as $|\psi_{50}| \gg |\psi_{l,crit}| > |\text{operating } \psi_l|$. Atmospheric conditions and soil water states are assumed to define the prevailing conditions for all leaves and absorbing roots, respectively.

When $\text{PPFD} > 0$, photosynthesis commences, assimilated sugars that accumulate in the mesophyll are first transported to the companion cell and subsequently to the sieve elements in the loading zone (i.e., leaf). Loading is achieved by either active (i.e., polymer trapping and apoplastic pumping) or passive (i.e., molecular diffusion) mechanisms (Turgeon, 2010). Passive loading is common in woody seed plants (i.e., angiosperm and gymnosperm), while many herbaceous species exhibit active loading (Jensen et al., 2016; Turgeon, 2010).

At the sub-hourly time-scale defined over a fixed period Δt , $f_c(\psi_l)$, $f_e(\psi_l)$, environmental factors (e.g., atmospheric forcing and soil water status) are assumed to be stationary. Hence, over such Δt period, production rate of sucrose (P_C) in the loading zone can be approximated by:

$$P_C = \frac{N_c}{\Delta t} \approx \alpha (\beta f_c A_l), \quad (6)$$

where N_c are the moles of sucrose produced in the mesophyll cells and then transported into the loading zone, and $\alpha (\in [0, 1])$ and β are the species-specific loading efficiency and the number of sucrose molecules produced from one assimilated CO_2 molecule ($\beta = 1/12$ for sucrose only), respectively. It must be noted that for a stationary photosynthetic rate, sucrose production (and subsequent transport) rate (i.e., P_C) is

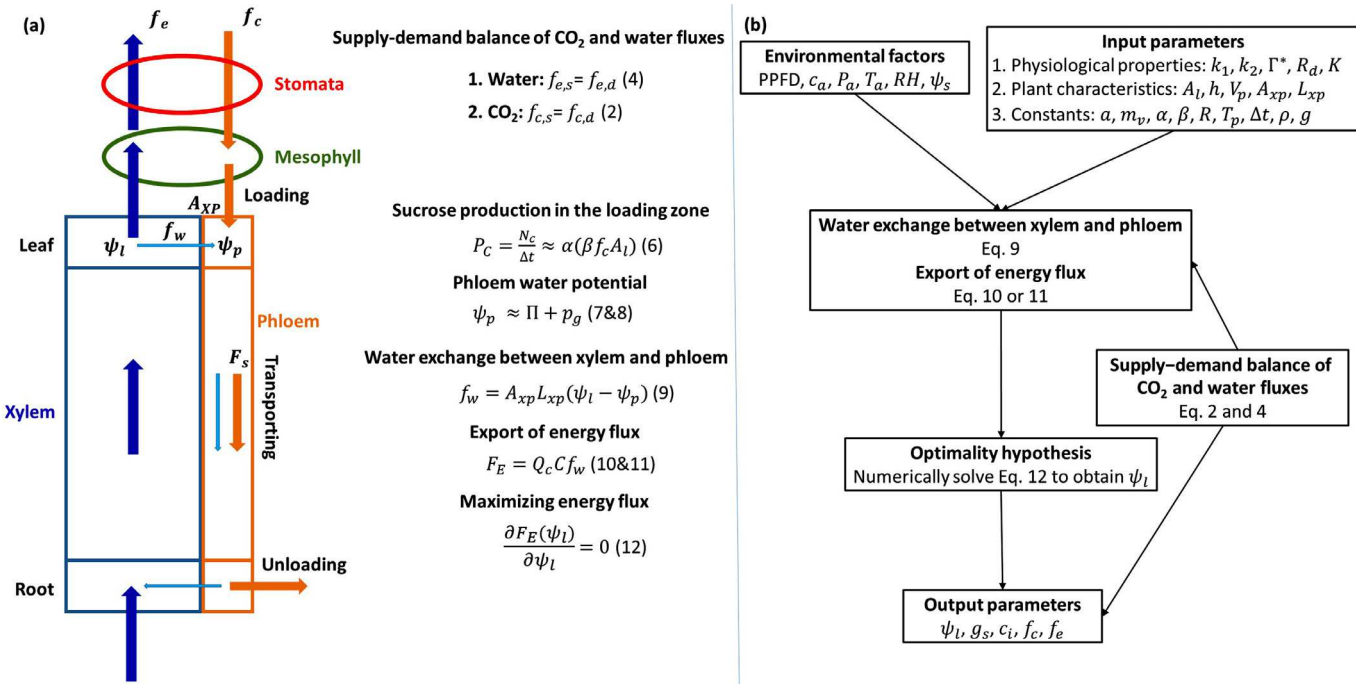


Fig. 2. (a) Schematic of the leaf-level gas exchange and the simultaneous water and sucrose mass fluxes in xylem and phloem. (b) Flowchart showing the numerical calculation process for the modeling system.

assumed to be constant. The α is set to be 1 when assuming that all the sucrose molecules assimilated from f_c enter the loading zone over a Δt period (i.e., no time delay for different sucrose loading mechanisms) (Hölttä et al., 2017; Nikinmaa et al., 2013). The total water potential (ψ_p) in the loading zone of the phloem includes turgor pressure (p_p), osmotic potential (Π) and gravitational potential ($p_g = \rho gh$ where ρ is the liquid density that varies weakly with N_c , g is the gravitational acceleration and h is the height above a datum set at the forest floor). The kinetic energy head is ignored as expected for low Reynolds number flows. Hence,

$$\psi_p = p_p + \Pi + p_g. \quad (7)$$

For an ideal solute and diluted sucrose concentration, the loading phloem sap Π can be computed from the van't Hoff formula (Campbell and Norman, 1998; Nobel, 2009) given by:

$$\Pi = -RT_p C, \quad (8)$$

where R is the gas constant, T_p is the absolute temperature of the loading phloem and $C = N_c/V_p$ is the sucrose concentration accumulated over Δt in the loading phloem volume (V_p). The magnitude of p_p is dictated by the elastic nature of sieve tubes and the amount of water stored in the loading phloem. That is, the relative change in V_p due to alternating shrinkage and swelling determines p_p (i.e., elastic pressure-volume curve). Over the short Δt , water storage in the loading phloem is also neglected and p_p may be ignored relative to Π (Jensen et al., 2016). The amount of water drawn from nearby xylem conduits per unit time (f_w) is then balanced by the water outflow from the loading phloem (i.e., no water storage). The f_w is determined from the water permeability (L_{xp}) and water potential gradient across the interface separating the xylem and phloem in the loading zone characterized by an area A_{xp} and is given by:

$$f_w = A_{xp} L_{xp} (\psi_l - \psi_p). \quad (9)$$

Thus, the export of sucrose mass (F_s) and its associated energy flux (F_E) driven by the accumulated sucrose molecules over a Δt period (i.e., N_c),

Eq. (6)) from the loading phloem can be determined by:

$$F_s = C f_w, \quad (10)$$

$$F_E = Q_c F_s,$$

where Q_c (= 5637.86 kJ mol⁻¹) is the energy content of sucrose. Eq. (10) considers only advective and neglects diffusive (and dispersive) effects as well as any sucrose leaks (i.e. no loss in N_c over Δt in the loading phloem). Previous studies have reported that phloem sap speed mainly depends on sieve element geometry (Jensen et al., 2011; Mullendore et al., 2010) instead of plant height (i.e., the whole path of sucrose flow throughout phloem) (Dannoura et al., 2011; Liesche et al., 2015; Windt et al., 2006). Modeling analysis (Christy and Ferrier, 1973; Thompson and Holbrook, 2003) also indicated that the water influx from xylem to phloem in the leaf is the main driver responsible for sucrose transport. It is for these reasons that the aforementioned assumptions may not be too restrictive in natural settings (Jensen et al., 2016). However, it is to be noted that F_E does not represent the actual instantaneous export of energy flux. Given the steady-state assumption here, Δt must also be sufficiently large to allow accumulation of N_c from mesophyll cells as needed to initiate phloem transport by osmosis. After osmosis is initiated, a pulse of energy (i.e., F_E) occurs that then can be used to determine the optimal g_s when F_E is maximized. Residual sucrose molecules from a previous Δt period in the loading cell are assumed to be negligible and do not impact F_E (or F_s). Naturally, Δt must also be sufficiently long to allow for the transport of sugar molecules from the mesophyll cells into the loading cell and subsequent buildup of N_c to initiate an osmo-regulated flux that exports sugars out of the loading cell. However, Δt must be sufficiently short so that f_c and g_s can be treated as stationary variables. Ideally, a non-steady state model that can accommodate transport processes of assimilated sugar from mesophyll to the companion cell and to the sieve elements in the leaf and to the sugar sinks (i.e., storage and unloading) throughout the plant (see Section 3.4) is required. Surrogating the effects of such unsteadiness to a pre-fixed (but constrained) Δt allows for the consideration of a quasi-steady model to be formulated for the instantaneous export of energy flux.

Table 1
Nomenclature.

Symbol	Description	Unit
A_l	Leaf area	m^2
A_{xp}	Contact area between xylem and phloem in the loading zone	m^2
a	Relative diffusivity of water vapor with respect to CO_2	Dimensionless
a_2	Photosynthetic parameters ($= K_c(1 + C_{oa}/K_o)$)	$\mu\text{mol mol}^{-1}$
C	Sucrose concentration in the loading phloem	mol m^{-3}
C_{oa}	Oxygen concentration in the atmosphere	mmol mol^{-1}
c_a	Atmospheric CO_2 concentration	ppm
c_i	Inter-cellular CO_2 concentration	ppm
D	Vapor pressure deficit	kPa
D_0	Normalizing constant in Leuning model	kPa
E	Energy gain in Eq. (11)	mol s^{-1}
E_c	Limiting energy cost in Eq. (11)	mol s^{-1}
E_{\max}	Maximum permissible energy gain in Eq. (11)	mol s^{-1}
F	Reduction function BWB and LEU models	Dimensionless
F_E	Export of energy flux from the loading phloem	kcal s^{-1}
F_s	Export of sucrose flux from the loading phloem	mol s^{-1}
$F_{E, ww}$	F_E under well-watered soil condition	kcal s^{-1}
f_w	Amount of water drawn from nearby xylem conduits to loading phloem per unit time	$\text{m}^3 \text{ s}^{-1}$
$f_{c, d}$	Biochemical demand for CO_2	$\mu\text{mol m}^{-2} \text{ s}^{-1}$
$f_{c, s}$	Supply of CO_2 flux from the atmosphere	$\mu\text{mol m}^{-2} \text{ s}^{-1}$
$f_{c, \max}$	Maximum assimilation rate ($= k_1 - R_d$) at $c_i \rightarrow \infty$	$\mu\text{mol m}^{-2} \text{ s}^{-1}$
f_c	Leaf-level assimilation rate	$\mu\text{mol m}^{-2} \text{ s}^{-1}$
$f_{c, crit}$	Maximum permissible assimilation rate	$\mu\text{mol m}^{-2} \text{ s}^{-1}$
f_e	Leaf-level transpiration rate	$\text{mol m}^{-2} \text{ s}^{-1}$
$f_{e, d}$	Evaporative demand	$\text{mol m}^{-2} \text{ s}^{-1}$
$f_{e, s}$	Water supply function	$\text{mol m}^{-2} \text{ s}^{-1}$
$f_{e, crit}$	Maximum permissible water transport capacity	$\text{mol m}^{-2} \text{ s}^{-1}$
g	Gravitational acceleration	m s^{-2}
g_s	Stomatal conductance	$\text{mol m}^{-2} \text{ s}^{-1}$
$g_{s, crit}$	Maximum permissible stomatal conductance	$\text{mol m}^{-2} \text{ s}^{-1}$
g_b	Boundary-layer conductance	$\text{mol m}^{-2} \text{ s}^{-1}$
g_m	Mesophyll conductance	$\text{mol m}^{-2} \text{ s}^{-1}$
$g_{s, ww}$	g_s under well-watered-soil condition	$\text{mol m}^{-2} \text{ s}^{-1}$
$g_{s, ref}$	Referenced conductance at $D = 1 \text{ kPa}$	$\text{mol m}^{-2} \text{ s}^{-1}$
$H_{a, L}$	Hamiltonian for conventional SOT	$\mu\text{mol m}^{-2} \text{ s}^{-1}$
$H_{a, X}$	Hamiltonian for modified SOT	$\mu\text{mol m}^{-2} \text{ s}^{-1}$
h	Height of the leaf	m
J	Electron transport rate	$\mu\text{mol m}^{-2} \text{ s}^{-1}$
K	Whole-system conductance	$\text{kg s}^{-1} \text{ MPa}^{-1}$
K_{\max}	Maximum whole-system conductance	$\text{kg s}^{-1} \text{ MPa}^{-1}$
$K_{s, max}$	Maximum leaf-specific tree conductance ($= K_{\max}/A_l$)	$\text{kg s}^{-1} \text{ m}^{-2} \text{ MPa}^{-1}$ or $\text{mmol m}^{-2} \text{ s}^{-1} \text{ MPa}^{-1}$
K_c	Michaelis constants for CO_2 fixation	$\mu\text{mol mol}^{-1}$
K_o	Michaelis constants for oxygen inhibition	mmol mol^{-1}
k_1	Photosynthetic parameters ($= J/4$)	$\mu\text{mol m}^{-2} \text{ s}^{-1}$
k_2	Photosynthetic parameters ($= k_1 a_2/V_{c, \max}$)	$\mu\text{mol mol}^{-1}$
L_{xp}	Water permeability between xylem and phloem in the loading zone	$\text{m Pa}^{-1} \text{ s}^{-1}$
m	Stomatal sensitivity to D ($= [dg_s/d\ln(D)]/g_{s, ref}$)	Dimensionless
m_E	Empirical parameter linking g_s to f_c/c_a in BWB and LEU models	Dimensionless
m_w	Molecular weight of water	kg mol^{-1}
N_c	Number of sucrose molecules	μmol
PPFD	Photosynthetically active radiation	$\mu\text{mol m}^{-2} \text{ s}^{-1}$
P	Energy profit in Eq. 11	mol s^{-1}
P_a	Atmospheric pressure	kPa
P_p	Phloem turgor (or mechanical) pressure	MPa
p_g	Gravitational potential	MPa
Q_c	Energy content of sucrose	kJ mol^{-1}
R	Gas constant	$\text{J K}^{-1} \text{ mol}^{-1}$
R_d	Daytime mitochondrial respiration rate	$\mu\text{mol m}^{-2} \text{ s}^{-1}$
RH	Relative humidity	%
T_a	Air temperature	°C
T_p	Absolute temperature of the loading phloem	K
V_p	Volume of loading phloem	m^3
$V_{c, \max}$	Maximum carboxylation capacity	$\mu\text{mol m}^{-2} \text{ s}^{-1}$
Γ^*	CO_2 compensation point in the absence of mitochondrial respiration	$\mu\text{mol mol}^{-1}$
Π	Phloem osmotic potential	MPa
λ_L	Marginal water use efficiency for conventional SOT	$\mu\text{mol mol}^{-1}$
λ_X	Marginal water use efficiency for modified SOT	$\mu\text{mol mol}^{-1}$
λ_P	Long-term cost of maintaining transpirational stream relative to maintaining photosynthetic protein to support assimilation (Prentice et al., 2014)	$\mu\text{mol mol}^{-1}$
ψ_l	Leaf water potential in the xylem	MPa
ψ_s	Soil water potential	MPa
ψ_p	Total water potential in the loading phloem	MPa

(continued on next page)

Table 1 (continued)

Symbol	Description	Unit
$\psi_{l, crit}$	Leaf water potential at $f_{e, crit}$	MPa
ψ_{12}	Air-entry point	MPa
ψ_{50}	Leaf water potential at which hydraulic conductivity drops by 50%	MPa
α	Species-specific loading efficiency ($\in (0, 1)$)	Dimensionless
β	Number of sucrose molecules produced from one assimilated CO_2 molecule ($= 1/12$)	Dimensionless
Δt	Hourly time scale	s
ρ	Liquid density in the phloem	kg m^{-3}

When combining Eqs. (2), (4), (6)–(10) (see Appendix A), F_E to be maximized can now be expressed as a function of ψ_l and is given as:

$$\underbrace{F_E(\psi_l)}_{\text{Energy profit } (P)} = G \left[\underbrace{f_c^2(\psi_l)}_{\text{Energy gain } (E)} + \underbrace{I(\psi_l - p_g)f_c(\psi_l)}_{\text{Limiting cost } (E_c)} \right], \quad (11)$$

where $G = Q_c A_{xp} L_{xp} RT_p (\alpha \beta A_l \Delta t / V_p)^2$ and $I = (V_p / A_l) (\alpha \beta \Delta t R T_p)^{-1}$ are constants (i.e., independent of ψ_l) associated with phloem system properties. The F_E here has a unit of joule per time and represents the energy profit due to the addition of sucrose molecules arising from f_c^2 supplied by the atmosphere over a Δt period. The first term on the right-hand side represents the energy gain ($E = f_c^2(\psi_l)$) but is constrained by the soil-xylem hydraulic system for a given ψ_s (see Eqs. (2) and (4)). This constraint arises because the solutions of $\partial f_c / \partial g_s \times \partial g_s / \partial \psi_l = 0$ and $\partial f_e / \partial g_s \times \partial g_s / \partial \psi_l = 0$ are the same. As ψ_l decreases with increasing g_s , a larger energy gain is achieved until the maximum permissible energy gain ($E = E_{\max}$) is reached at $\psi_{l, crit}$. However, the decrease in ψ_l also impedes f_w that drives F_E (see Eqs. (9) and (10)). This mechanism, which represents an additional cost of energy (E_c) due to interaction between xylem and phloem in the loading leaf, is the physical significance of the second term on the right-hand side of Eq. (11). The E_c is always a cost term because the value of $(\psi_l - p_g)$ is never positive. When the drop in ψ_l reaches a certain threshold ($\psi_{l, opt}$) expected to occur before $\psi_{l, crit}$, the increase in energy gain is no longer larger than the increase in the limiting cost, implying diminishing returns of energy profit (P) in the system. The optimal $\psi_{l, opt}$ that ensures a maximum P (i.e., F_E) can now be determined by setting

$$\frac{\partial F_E(\psi_l)}{\partial \psi_l} = 0, \quad (12)$$

when $\partial^2 F_E(\psi_l) / \partial \psi_l^2 < 0$. As shown in Fig. 2(b), $\psi_{l, opt}$ (i.e., operating ψ_l) is numerically solved through Eq. (12) for a given set of environmental factors, physiological properties, plant characteristics and constant parameters. The corresponding g_s , c_p , f_c and f_e can be computed from Eqs. (2) and (4). Eq. (12) sets the optimal criterion that reflects the energetics of the evolution principle (Lotka, 1922), in which the energy flux is maintained efficient (maximum) at current state when the system is explicitly subjected to the limiting constraints through the transport or physiological processes. A favorable plant body that can enhance larger energy flux through the system may be further promoted by the maximum input of energy flux. The points of departure from the conventional SOT or profit-maximization are that (1) the *Gain* in the objective function here is proportional to f_c^2 (not f_c); and (2) the *Cost* is directly derived (not externally assumed) from the limiting constraints imposed on the system and arises from xylem-leaf-phloem interaction. In the present modeling framework, however, a number of mechanisms (e.g., adjustments in mesophyll conductance and osmotic regulation with different soil water status) that may potentially impact the transport system and subsequently the *Gain* and *Cost* are not considered but discussed later in Section 3.4. We now show that the proposed approach recovers the form of objective function (i.e., *Gain-Cost* where *Gain* and *Cost* are linearly proportional to f_c and f_e or a function of ψ_l , respectively) in the conven-

tional SOT and profit-maximization that predict g_s for well-watered soil condition.

2.2. Recovery of prior formulations for well-watered soil conditions

Because prior g_s formulations have been shown to describe a large corpus of data (especially under well-watered conditions), it is assumed that their mathematical form offers a compact representation of all such experiments. When the soil moisture content is near saturation (i.e., $|\psi_s| < < |\psi_l|$) and the operating $|\psi_l|$ for plants shorter than $c. 20$ m is much larger than p_g at high f_e (Manzoni et al., 2013a), Eq. (11) can be further simplified to (see Appendix A)

$$F_{E,ww}(\psi_l) = G \left[f_c^2(\psi_l) - m_v I A_l \frac{f_e(\psi_l)}{K(\psi_l)} f_c(\psi_l) \right], \quad (13)$$

where the energy profit $F_{E,ww}$ is defined for well-watered conditions. Again, the optimal $\psi_{l, opt}$ can be obtained by setting $\partial F_{E,ww} / \partial \psi_l = 0$ that then yields:

$$\frac{\partial f_c(\psi_l)}{\partial \psi_l} - \frac{m_v I A_l}{2} \left[\underbrace{\frac{f_e(\psi_l)}{K(\psi_l)} f_c(\psi_l)}_{\mathbf{M}} \frac{\partial f_c(\psi_l)}{\partial \psi_l} + \underbrace{\frac{\partial}{\partial \psi_l} \left(\frac{f_e(\psi_l)}{K(\psi_l)} \right)}_{\mathbf{N}} \right] = 0. \quad (14)$$

A scaling analysis featured in Appendix B compares the two contributions, labeled M and N, in Eq. (14). The outcome of this analysis shows smaller contribution of term M when compared with term N. This finding may have been anticipated for well-watered soil conditions because the reduction in K is usually small at $\psi_s \approx 0$ when stomatal closure commonly occurs before the air-entry point (i.e., at ψ_l where 12% of K losses occur) (Bond and Kavanagh, 1999; Sparks and Black, 1999). Based on this scaling analysis, Eq. (14) can be further simplified to:

$$\frac{\partial}{\partial \psi_l} \left[f_c(\psi_l) + \frac{I}{2} \psi_l \right] = 0, \quad (15)$$

or

$$\frac{\partial}{\partial \psi_l} \left[f_c(\psi_l) - \underbrace{\frac{V_p m_v}{2 \alpha \beta K_{\max} \Delta t R T_p} f_e(\psi_l)}_{\lambda_X} \right] = 0. \quad (16)$$

Interestingly, Eqs. (15) and (16) converge respectively to the profit-maximization (Wolf et al., 2016) and to the modified SOT (Eq. (5)). This convergence suggests a tight connection between the leaf-xylem-phloem system given the **dissimilarity** in objective functions. The emergence of a linear relation between g_s and ψ_l for a nearly constant K_{\max} at $\psi_s \approx 0$ (see Eq. (4)) also results in the convergence of the conventional and modified SOT's: $\partial H_{a,L}(g_s) / \partial g_s = 0$ is equivalent to $\partial H_{a,X}(\psi_l) / \partial \psi_l = 0$ and $\lambda_L = \lambda_X$. One of the main novelties here is the predicted dependency of λ_X (or λ_L) on xylem and phloem properties arising from the condition $\partial F_{E,ww} / \partial \psi_l = 0$. The analysis may also indicate why the time-scale used for SOT to predict g_s remains uncertain (Buckley et al., 2016). Current uncertainty in determining λ_X arises from the inexact specification of Δt . Again, a non-steady state model is needed to eliminate the dependency of λ_X (or λ_L) on Δt .

An analytical solution for the proposed approach (i.e., Eq. (16)) can now be derived under some conditions. Assuming $f_c \gg R_d$, $c_i \gg \Gamma^*$, the optimal g_s and c_i/c_a are given as (see Appendix C):

$$g_{s,ww} = \left(1 + \sqrt{\frac{k_2 + \Gamma^*}{aD\lambda_X}} \right) \frac{f_c}{c_a},$$

$$\frac{c_i}{c_a} = \frac{\sqrt{\frac{k_2 + \Gamma^*}{a\lambda_X}}}{\sqrt{\frac{k_2 + \Gamma^*}{a\lambda_X} + \sqrt{D}}}. \quad (17)$$

The link between the xylem, phloem, and leaf is provided here by λ_X (see Eq. (16)). When f_c operates under RuBP limitation, Eq. (17) converges to the form of g_s derived from conventional SOT proposed elsewhere (Medlyn et al., 2011). If the higher order terms in the Taylor series expansion expressing c_i/c_a are neglected, as shown in Appendix C, the optimal g_s and c_i/c_a simplify to:

$$g_{s,ww} = \sqrt{\frac{k_2 + \Gamma^*}{a\lambda_X}} \frac{f_c}{c_a} D^{-1/2},$$

$$\frac{c_i}{c_a} = 1 - \sqrt{\frac{a\lambda_X}{k_2 + \Gamma^*}} \sqrt{D}. \quad (18)$$

Eq. 18 also recovers the linear dependency of g_s on f_c/c_a as in BWB and LEU models and suggests that m_E encodes the xylem-phloem system properties. Also, the predicted c_i/c_a varies marginally with D as has been known for some time now (Wong et al., 1979). Eq. (18) also recovers the form of optimal g_s and c_i/c_a derived by others (Katul et al., 2010; 2012; Volpe et al., 2011) when a linearized biochemical demand function is assumed (as expected for Rubisco limitations on f_c). The convergence of analytical solutions here can be expected when they are all derived from the same objective function (i.e., Eq. (16)) for well-watered condition. These analytical solutions mainly differ in the choice of RuBP or Rubisco limitations (i.e., limitation regime is known) on f_c that can be bypassed when co-limitation (i.e., Eq. (1)) is accounted for (Vico et al., 2013). Neglecting Γ^* and R_d may generate unrealistic g_s responses at low c_a although this assumption may not be too restrictive especially when c_a is expected to increase above current level (i.e., > 400 ppm). However, these analytical solutions are invalid under water stress condition unless variations in λ_X with ψ_s can be appropriately described (Manzoni et al., 2011).

As suggested elsewhere (Prentice et al., 2014), the optimal g_s and c_i/c_a under Rubisco-limitation can be assumed to operate with minimum maintenance cost that simultaneously maximizes f_c and f_e and are given as:

$$g_{s,ww} = \left(1 + \sqrt{\frac{a_2}{aD\lambda_p}} \right) \frac{f_c}{c_a},$$

$$\frac{c_i}{c_a} = \frac{1}{1 + \sqrt{\frac{a\lambda_p}{a_2}} \sqrt{D}}, \quad (19)$$

where λ_p is the long-term cost of maintaining transpirational stream relative to maintaining photosynthetic protein to support assimilation. Again, the current approach recovers similar forms of g_s and c_i/c_a to Eq. (19) and the dependency of the apparent λ_p on K_{max}^{-1} is also reflected by λ_X analytically derived here. This dependency of λ_X on K_{max}^{-1} has been inferred by fitting SOT to a numerical model with consideration of whole-plant sucrose transporting length (Hölttä et al., 2017). The effects of drying soil process on g_s is embedded in a/b ($= \lambda_p \sim K^{-1}$) in Prentice et al. (2014) that is equivalent to λ_X in SOT while the increase

Table 2

Physical characteristics of needle samples adopted elsewhere (Domec et al., 2016b) and anatomical attributes of phloem for the loading leaf of *Pinus taeda* L. growing under ambient- $^{a}\text{CO}_2$ and elevated- $^{e}\text{CO}_2$ conditions at Duke-FACE site.

	A_n (mm ²)	L_n (cm)	d_p (μm)	N_p
$^{a}\text{CO}_2$	0.50	17.4	5.75	330
$^{e}\text{CO}_2$	0.48	18.0	5.58	276

A_n : needle cross-sectional area; L_n : needle length ; d_p : diameter of phloem cell; N_p : number of phloem cells per needle.

in the carbon cost represented as a function of ψ_l (i.e., $\theta(\psi_l)$) with decreasing ψ_l is assumed in Wolf et al. (2016). The modeling approaches proposed by Prentice et al. (2014) and Wolf et al. (2016) can accommodate how g_s is impacted by the reduction in K as drought progresses but may not reflect the isohydric-to-anisohydric behavior that can be explained by the energy partitioning between P , E and E_c in Eq. (11) (see Section 3.2). In the absence of drought stress, the convergence of various optimization goals shown here invites the use of the energetics of the evolution principle as a unifying hypothesis to predict g_s .

3. Results and discussion

To address the study objectives, we first analyze how different transport and physiological processes impact the short-term g_s responses to environmental factors through model calculations featured in Section 3.1. In particular, we first examine the sensitivity of g_s to D and ψ_l that has been well documented in the literature. In Section 3.2, we then explore how the difference in the coordinated leaf-xylem-phloem system determines different water use strategies among plants (i.e., isohydric-to-anisohydric behavior) during a soil dry-down process. The analysis here is accomplished by examining how the difference in the soil-xylem hydraulics impact the energy partitioning in Eq. (11) (i.e., P , E and E_c) and hence the sensitivity of ψ_l to ψ_s and D . We also explain the general decreasing trends in g_s following elevated atmospheric CO_2 concentration sustained over long time-scales in Section 3.3. Specifically, how the adjustments in plant hydraulic and physiological properties in response to a new stationary CO_2 concentration level modify the value of λ_X dictating leaf-level gas exchange is explored. Finally, we briefly summarize the study limitation in the present modeling framework in Section 3.4. For all the following model calculations (i.e., model base case), the physiological, hydraulic and allometric attributes of soil-plant system for coniferous species in general reported elsewhere (Huang et al., 2017) are adopted. Physical characteristics of leaves and anatomical attributes of phloem for *Pinus taeda* L. listed in Table 2 are used.

3.1. Stomatal responses to variations in environmental conditions

To illustrate a number of features of the new g_s model, the focus now is on g_s responses to short-term (sub-daily) variations in environmental factors. It is assumed that at sub-daily time-scales, the hydraulic and physiological properties of plants remain constant. The proposed approach to g_s captures the main features of stomatal responses to key environmental factors including PPFD, c_a , D , T_a and ψ_s (Fig. 3). The overall negative trends in g_s with respect to increasing D (Aphalo and Jarvis, 1991; Ball and Farquhar, 1984; Farquhar et al., 1980a; Grantz, 1990; Katul et al., 2009; Lange et al., 1971; Lendzion and Leuschner, 2008; Massman and Kaufmann, 1991; McAdam and Brodribb, 2015; Monteith, 1995; Morison and Gifford, 1983; Oren et al., 1999; Schulze et al., 1974) and decreasing ψ_s (Berninger et al., 1996) are governed by the supply-demand balance of water flux (i.e., Eq. (4)) that presets the maximum permissible stomatal conductance ($g_{s,crit}$) and subsequently E_{max} in Eq. (11) at $\psi_{l,crit}$. To examine the sensitivity of predicted g_s to D , the empirical relation between g_s and D (Oren et al., 1999) is adopted

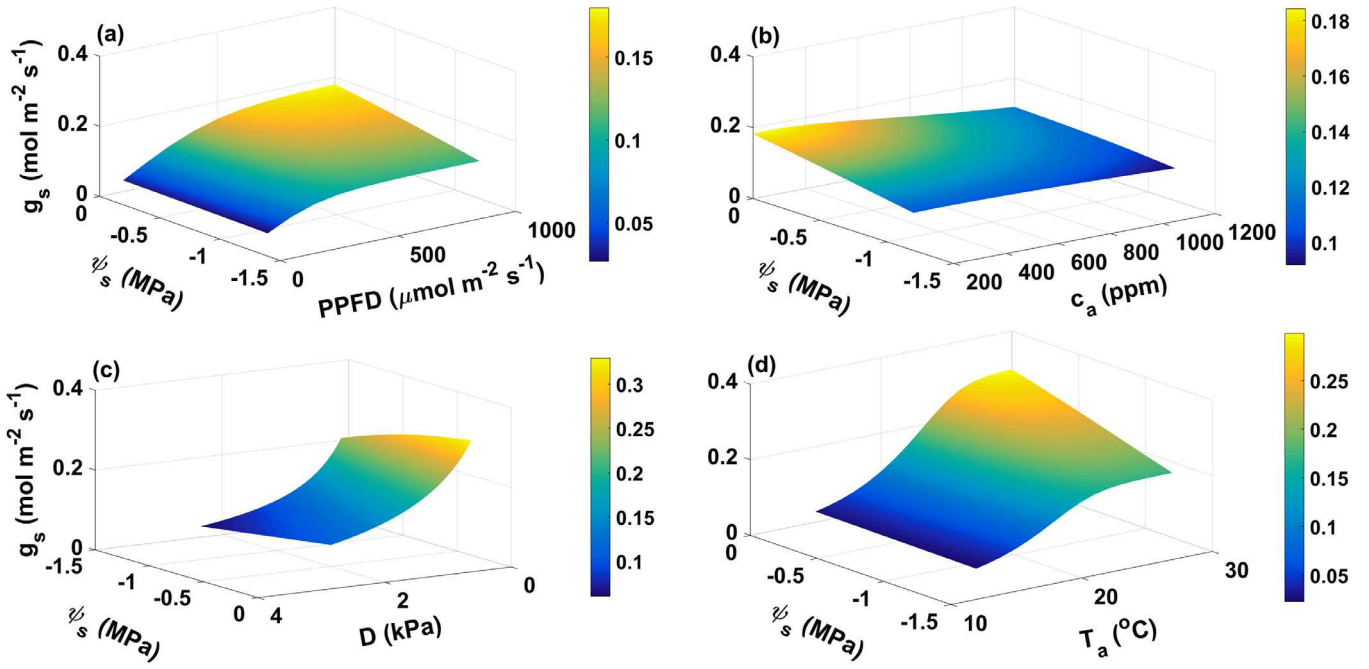


Fig. 3. Modeled stomatal conductance (g_s) as a function of soil water potential (ψ_s) and (a) photosynthetically active radiation (PPFD), (b) atmospheric CO₂ concentration (c_a), (c) vapor pressure deficit (D) and (d) air temperature (T_a). All the model parameters used here are the same as Fig. 1. PPFD, T_a , c_a and RH are respectively fixed to be $1000 \mu\text{mol m}^{-2} \text{s}^{-1}$, 25°C , 400 ppm and 50% in general while PPFD varies from 100 to $1000 \mu\text{mol m}^{-2} \text{s}^{-1}$ in (a), c_a varies from 200 to 1200 ppm in (b), RH varies from 10 to 80% in (c), and T_a varies from 15 to 30°C with a fixed $D = 1 \text{ kPa}$.

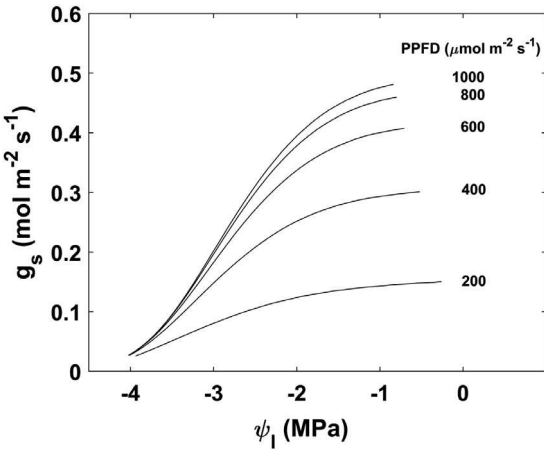


Fig. 4. Modeled stomatal conductance (g_s) as a function of leaf water potential (ψ_l) for different photosynthetically active radiation (PPFD) with a range from 200 to $1000 \mu\text{mol m}^{-2} \text{s}^{-1}$. All the model parameters used here are the same as Fig. 1. The air temperature (T_a), atmospheric CO₂ concentration (c_a) and relative humidity (RH) are respectively set to be 25°C , 400 ppm and 90% .

as it encodes a large corpus of leaf and sapflow data. This expression is given as:

$$g_s = g_{s,\text{ref}} [1 - m \times \ln(D)], \quad (20)$$

where $g_{s,\text{ref}}$ is the reference conductance at $D = 1 \text{ kPa}$ and m is the ratio of $dg_s/d\ln(D)$ to $g_{s,\text{ref}}$. Using all the model runs in Fig. 3(c), the value of m determined by least-square fit to Eq. (20) is 0.61 and is close to the value (i.e., 0.59) derived from a meta-analysis of $c. 30$ species (Oren et al., 1999). When ψ_s decreases, the predicted relation between g_s and ψ_l (Fig. 4) also recovers a Weibull-type form that has been globally observed (Klein, 2014). This Weibull-type $g_s - \psi_l$ relation is mainly dictated by the shape of $K(\psi_l)$ (i.e., soil-xylem hydraulics) without relying on a pre-specified ψ_l -dependent λ_X (Manzoni et al., 2011) or any cost

function linked with xylem hydraulics (Wolf et al., 2016) formulated in SOT or profit-maximization. The predicted $c_i/c_a = 0.82 \pm 9.8\%$ across all runs for well-watered soil condition in Fig. 3, representing a relatively conservative c_i/c_a when compared with g_s , f_c , f_e and ψ_l . This predicted near-constant c_i/c_a is supported by previous studies ($c_i/c_a = 0.6 - 0.9$) (Drake et al., 1997; Ehleringer and Cerling, 1995; Prentice et al., 2014; Wong et al., 1979). Based on a constant c_i/c_a , the general trends in negative stomatal response to c_a (Mansfield et al., 1990; Messinger et al., 2006; Morison, 1998; Morison and Gifford, 1983; Mott, 1988) and positive stomatal response to PPFD and T_a (Schulze et al., 1974; Wong et al., 1979) are mainly reflected by the supply-demand balance of CO₂ flux.

3.2. Coordinated photosynthetic-hydraulic-sucrose transporting machinery explaining isohydric-to-anisohydric behavior

The analysis is now expanded to examine the coordinated photosynthetic-hydraulic-sucrose transporting machinery in species with different water use strategies across the spectrum of isohydric-to-anisohydric behavior as drought progresses.

3.2.1. General features of isohydric-to-anisohydric behavior and the model set-up

The isohydric-to-anisohydric behavior is mainly defined by the sensitivity of ψ_l to ψ_s and D (Martínez-Vilalta and Garcia-Forner, 2017). The general features differentiating isohydric and anisohydric behavior (Domec and Johnson, 2012; Meinzer et al., 2016) are that (1) isohydric species tend to maintain a relatively constant midday ψ_l that is less sensitive to decreasing ψ_s and increasing D ; (2) anisohydric species allow midday ψ_l to significantly decrease with decreasing ψ_s and increasing D such that a relatively larger f_e and f_c can be maintained when compared to isohydric species. Studies conducted to contrast isohydric and anisohydric behavior (Kolb and Sperry, 1999; McDowell et al., 2008; Schultz, 2003; Sperry et al., 1998; 2002) reported that species with larger ψ_{12} (i.e., air-entry point that is commonly defined at ψ_l where 12% of K losses occur) tend to exhibit more isohydric behavior while anisohydric behavior occurs in species with a smaller ψ_{12} . The proposed model is

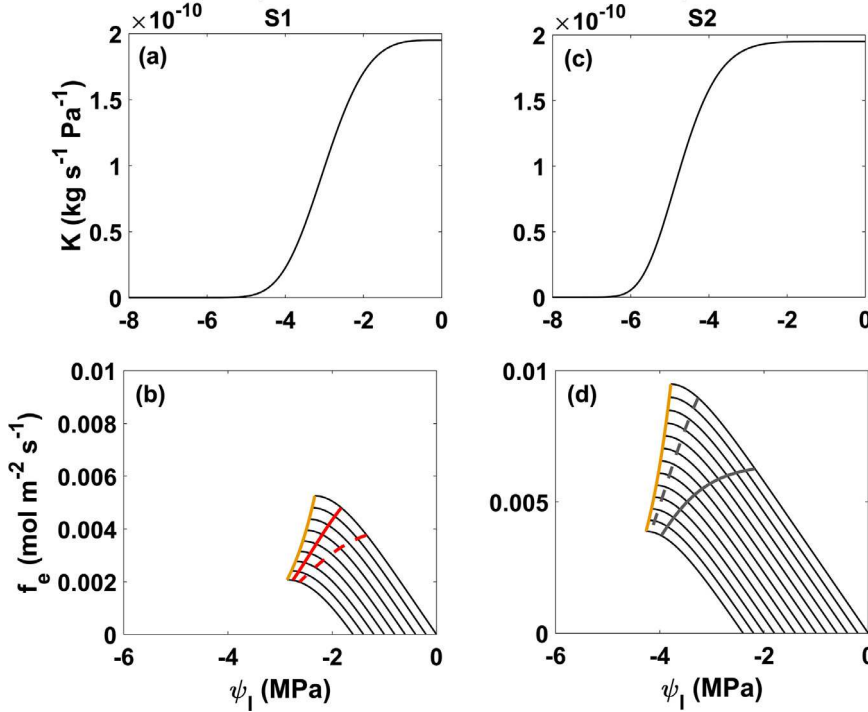


Fig. 5. (a) Whole-system hydraulic conductance (K) as a function of total leaf water potential (ψ_l) for scenario 1 (S1). (b) Water supply function for S1 determined by K and ψ_l for different soil water potential (ψ_s) with maximum permissible transpiration rate ($f_{e, crit}$; orange solid line) and predicted transpiration rate (f_e ; red solid line). All the model parameters used in (a) and (b) are the same as Fig. 1. The photosynthetically active radiation (PPFD), air temperature (T_a), atmospheric CO_2 concentration (c_a) and relative humidity (RH) are respectively set to be $1200 \mu\text{mol m}^{-2} \text{s}^{-1}$, 25°C , 400 ppm and 50% . The range of ψ_s is from 0 to -1.6 MPa . For S1, the predicted f_e with $RH = 80\%$ is shown (red dashed line). (c) and (d) are the same as (a) and (b) but for a smaller air-entry point (ψ_{12}) where a nearly constant maximum conductance (K_{\max}) can operate represented as scenario 2 (S2). The range of ψ_s is from 0 to -2.4 MPa . $f_{e, crit}$ and predicted f_e in S2 are respectively represented by orange and gray solid lines. For S2, the predicted f_e with 50% increases in maximum carboxylation capacity and light saturated rate of electron transport is shown (gray dashed line). (For interpretation of the references to color in this figure legend, the reader is referred to the web version of this article.)

now shown to be able to reconcile connections between ψ_{12} and the defining features of isohydric-to-anisohydric.

For this reason, two scenarios (S1 with larger ψ_{12} and S2 with smaller ψ_{12}) are now constructed to illustrate how the magnitude of ψ_{12} modifies the leaf-xylem-phloem system and impacts isohydric-to-anisohydric behavior during reduced soil moisture conditions (Fig. 5). All the model parameters used for S1 are the same as the model base case. A smaller ψ_{12} is selected for S2 but all other model parameters are maintained the same as S1. The plant hydraulic and physiological properties are assumed to be constant (i.e., no acclimation or adaptation) during a soil dry-down process. The environmental factors (i.e., PPFD, T_a , c_a , RH and ψ_s) used in the model runs are maintained the same for S1 and S2. The model results (i.e., predicted f_e , E/E_{\max} , E_c/E_{\max} and P/E_{\max}) for the two cases are respectively represented as red and gray solid lines for S1 and S2 in Figs. 5 and 6. For S1, a larger RH is also used in another model run to examine if a reduced D can modify isohydric-to-anisohydric behavior, as represented by red dashed lines in Figs. 5 and 6. For S2, we also use a larger photosynthetic capacity (i.e., larger k_1 and k_2) to explore the effects of relative magnitude of photosynthetic capacity in relation to the water transport capacity on the isohydric-to-anisohydric behavior, as represented by gray dashed lines in Figs. 5 and 6. Specifically, it is shown that maximizing the energy profit P across these two different ψ_{12} scenarios recovers the key features delineating isohydric from anisohydric behavior. For simplicity, it is assumed that K_{\max} maintains a near-constant value as loss of conductivity at ψ_{12} is assumed to be minor ($\sim 12\%$).

3.2.2. Linkage between the energy partitioning in Eq.(11) and the sensitivity of f_e and ψ_l to ψ_s and D

As g_s increases monotonically with decreasing ψ_l (up to $\psi_{l, crit}$), E_{\max} occurs at $f_{e, crit}$ and can be surrogated to a preset $f_{e, crit}$ for a given ψ_s .

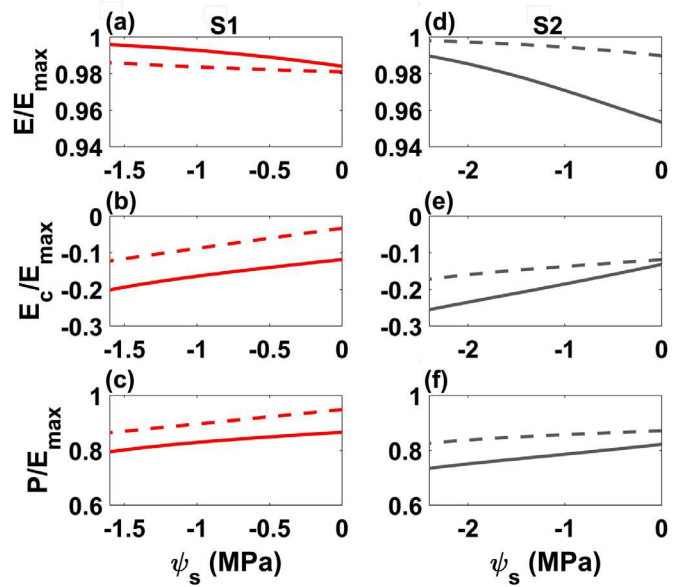


Fig. 6. The energy partitioning in Eq. (11) for the two scenarios (S1 and S2). The energy gain (E), limiting cost (E_c) and energy profit (P) relative to maximum permissible energy gain (E_{\max}) as a function of soil water potential (ψ_s) are respectively shown in (a), (b) and (c) for S1. The model results for $RH = 50\%$ and 80% are respectively represented by the red solid and dashed lines. (d), (e) and (f) are the same as (a), (b) and (c) but for S2. Same as Fig. 5(d), model results for 50% increases in maximum carboxylation capacity and light saturated rate of electron transport are represented by gray dashed lines. (For interpretation of the references to color in this figure legend, the reader is referred to the web version of this article.)

The E_{\max} is constrained by the soil-xylem limitation (see Eq. (11) and Section 1.2). However, the corresponding $\psi_{l, crit}$ does not guarantee a maximum P due to finite E_c as discussed in Section 2.1. In Eq. (11), maximum P occurs at $\psi_{l, opt} (> \psi_{l, crit})$ and the corresponding predicted f_e or f_c can be used as an indicator for the actual level of E . Thus, the energy partitioning between P , E and E_c in Eq. (11) (Fig. 6) can be used to explain the sensitivity of f_e and ψ_l to ψ_s and D that then determines isohydric-to-anisohydric behavior.

3.2.3. Similar behavior of isohydric and anisohydric plants under severe drought condition

The common feature of the two scenarios is that the difference between $f_{e, crit}$ (i.e., orange lines in Fig. 5(b) and (d)) and predicted f_e (Δf_e) decreases as drought progresses. This decreasing trend in Δf_e is reflected by the increasing trend in E/E_{\max} up to nearly unity, implying that soil-xylem limitation dominates P at a small ψ_s . However, $\partial(E/E_{\max})/\partial\psi_s < 0$ does not suggest that E is enhanced by a smaller ψ_s . As ψ_s drops, the decrease in E ($\sim f_c^2$) is smaller than the decrease in E_{\max} ($\sim f_{c, crit}^2$) but P can be further suppressed by increasing E_c when severe drought conditions persist.

3.2.4. Isohydric and anisohydric behavior

When compared with S1, a smaller ψ_{12} in S2 allows a more negative operating ψ_l (i.e., anisohydric behavior) that further enhances the impediment of sucrose transport (i.e., E_c). The smaller E/E_{\max} in the case of S2 also suggests that the maximum permissible water transport capacity (i.e., $f_{e, crit}$) significantly overshoots the actual f_e required to attain the maximum P especially when $\psi_s \rightarrow 0$. This over-built soil-xylem hydraulics in S2 also permits a broader operating range of ψ_l in response to environmental factors such as D , PPFD and T_a . In the absence of water stress, it is advantageous to maintain maximum P and a larger f_c ($< f_{c, crit}$) although a larger f_e can be achieved by changes in environmental conditions (i.e., increasing D , PPFD or T_a). When compared with S2, Δf_e in the case of S1 is smaller due to a larger ψ_{12} (i.e., isohydric behavior; a narrower range of ψ_l where a nearly constant K_{\max} can operate). It is suggested that the main limiting component is the soil-xylem hydraulics, leading to smaller E_c and larger E/E_{\max} in S1. Although the maximum P , E_{\max} ($\sim f_{c, crit}^2$) and operating E ($\sim f_c^2$) in S1 are suppressed by a larger ψ_{12} , the limitation induced by the interaction between xylem and phloem in the loading leaf (i.e., E_c) is also reduced due to a larger operating ψ_l . However, if D in the case of S1 is reduced, the decrease in f_e (i.e., increase in ψ_l) results in a larger Δf_e (Fig. 5(b)) and smaller E/E_{\max} (Fig. 6(a)) where the enhancement in E_{\max} is larger than the enhancement in E . A reduced D also suppresses E_c due to the increase in ψ_l . This finding suggests that the maximum P and operating E can be enhanced even when the range of ψ_l is small (i.e., a larger ψ_{12}) for a nearly constant K_{\max} . Similar to S2, ψ_l in S1 can now respond to a wider range of D at short time-scale as a consequence of reduced f_e .

Hence, S1 and S2 may represent plant hydraulics associated with the more conservative and aggressive water use strategies for plants across the spectrum of isohydric-to-anisohydric behavior. However, the range of ψ_l for a nearly constant K_{\max} to operate (i.e., ψ_{12}) alone cannot be used to differentiate species with different water use strategy. To illustrate, Δf_e decreases with increasing photosynthetic capacity (i.e., larger k_1 and k_2 are used in S2), leading to a shift from anisohydric to isohydric behavior (i.e., narrower range of operating ψ_l along the gray dashed line) as shown in Fig. 5(d). A larger photosynthetic capacity also necessitates a larger f_e that reduces Δf_e and increases E/E_{\max} because soil-xylem hydraulics now dominate with a reduced contribution of E_c to P (gray dashed lines in Fig. 6(d), (e) and (f)).

To sum up, it is fair to state that the photosynthetic capacity for isohydric species has the tendency to nearly exploit $f_{e, crit}$ throughout a dry-down (i.e., $E/E_{\max} \rightarrow 1$). Isohydric plants are conservative water users (i.e., limited by soil-xylem hydraulics) but their photosynthetic capacity is aggressively utilizing the soil-xylem hydraulic system. Anisohydric plants, by contrast, are aggressive water users but they adopt

more conservative photosynthetic capacity that requires smaller f_e to maintain a maximum P compared to their $f_{e, crit}$ state. When responding to fluctuation in environmental conditions, the compartments of the system appear to operate in a coordinated manner so as to maintain P/E_{\max} without any apparent bottleneck even when ψ_s drops. While previous experimental studies mainly focused on the variation of ψ_l during a dry-down and the sensitivity of g_s to D and ψ_s to distinguish isohydric-to-anisohydric behavior (Domec and Johnson, 2012; Meinzer et al., 2016), the finding here forms a new model-generated hypothesis that has not been explored and requires testing in future field and laboratory experiments. That is, the magnitude of atmospheric aridity (i.e., D) and the relative magnitude of photosynthetic capacity in relation to the water transport capacity through soil-xylem hydraulic system can shift isohydric-to-anisohydric behavior.

3.3. Long-term effect of elevated atmospheric CO_2 concentration on leaf-level gas exchange

When plants acclimate or adapt to a changing environment, leaf-level gas exchange reflects concomitant adjustments in plant hydraulic and physiological properties. Under well-watered soil conditions, the closed form expressions for $g_{s, ww}$, f_c and water use efficiency (WUE = f_c/f_e) can be derived by replacing Eq. (17) into the supply-demand balance of CO_2 flux, and are given as:

$$\begin{aligned} g_{s, ww} &= \frac{k_1 \left(1 + \sqrt{\frac{k_2 + \Gamma^*}{aD\lambda_X}} \right)}{k_2 \left(1 + \sqrt{\frac{aD\lambda_X}{k_2 + \Gamma^*}} \right) + c_a}, \\ f_c &= \frac{k_1 c_a}{k_2 \left(1 + \sqrt{\frac{aD\lambda_X}{k_2 + \Gamma^*}} \right) + c_a}, \\ \text{WUE} &= \frac{c_a/aD}{1 + \sqrt{\frac{k_2 + \Gamma^*}{aD\lambda_X}}}. \end{aligned} \quad (21)$$

On long time-scales, xylem and phloem traits (i.e., λ_X) and photosynthetic parameters (i.e., k_1 and k_2) in Eq. (21) are shaped by the environmental conditions they have experienced. However, $g_{s, ww}$, f_c , WUE and c_i/c_a (i.e., Eq. (17)) represent short-term leaf-level responses to current states or environmental conditions. A large time-scale separation exists between variations in endogenous plant attributes (encoded in λ_X , k_1 and k_2) and instantaneous leaf-level responses (i.e., $g_{s, ww}$, f_c , WUE and c_i/c_a). For this reason, Eqs. (21) and (17) only focus on how measured modifications in λ_X following long-term elevated atmospheric CO_2 concentration modify photosynthetic parameters as well as $g_{s, ww}$, c_i/c_a ratio, f_c and WUE. For simplicity, the focus is on formulations that assume absence of water stress after the plants experience different c_a 's on long time-scales (e.g., by comparing leaves grown under ambient and enriched c_a conditions). Such a situation describes the setup for *Pinus taeda* L. growing under +200 ppm CO_2 above current level as reported from the Duke-Free Air CO_2 Enrichment (FACE) site. The Duke-FACE was conducted in a South-Eastern U.S. pine forest (Domec et al., 2009; 2016b; Tor-ngern et al., 2015) where leaf and plant hydraulic traits have been measured. When other environmental conditions are maintained the same, a reduced maximum leaf hydraulic conductance ($K_{leaf, max}$) was reported with increased c_a . In this case, the maximum leaf-specific tree conductance ($K_{s, max} = K_{max}/A_l$) decreased from 0.65 to 0.43 $\text{mmol m}^{-2} \text{s}^{-1} \text{MPa}^{-1}$ (Domec et al., 2016a) as a result of the reduction in $K_{leaf, max}$ (Domec et al., 2009). This general decrease in $K_{s, max}$ has been reported for ring-porous, diffuse-porous, coniferous and non-woody species in a literature survey conducted on elevated- CO_2 experiments over the last 40 years (Domec et al., 2016a). As shown in Table 2, the needle size, phloem diameter and the number of phloem cells per needle appear to be suppressed by increased atmospheric CO_2 . When

accounting for all the loading leaf at the canopy-level, the enhancement of canopy leaf area ($\sim 16\%$) (McCarthy et al., 2007) results in 35.6% decrease in K_{\max} but a nearly unaltered V_p (i.e., 5.8% decrease). Hence, the expenditure of water loss, λ_X , is predicted by Eq. (16) to increase by 65.1%, comparable with the percentage increase of λ_X (i.e., 62.9%) computed by inverting λ_X based on SOT from leaf-level gas exchange measurements at the same site (Katul et al., 2010). Furthermore, the difference in photosynthetic parameters of *Pinus taeda* L. between control- and elevated-CO₂ plots is not significant (Ellsworth et al., 2012; Katul et al., 2010). It was assumed here that acclimation of k_1 and k_2 did not occur (e.g., no down-regulation). If λ_X is the only plant trait to be modified by elevated-CO₂, the general trends in decreasing $g_{s,ww}$ and c_i/c_a ratio and increasing f_c and WUE with increasing c_a (Ellsworth et al., 2012; Katul et al., 2010) can be attributed to the combined effects of increasing λ_X and c_a (i.e., Eq. (21)). However, the suppression of $g_{s,ww}$ and c_i/c_a ratio by increasing λ_X is relatively small (Ellsworth et al., 2012; Katul et al., 2010) when compared with the sensitivity of f_c and WUE to long-term elevated-CO₂. The increment of c_a in the numerator of f_c and WUE further amplifies the effects of elevated-CO₂ on f_c and WUE.

3.4. Study limitation

Given all the assumptions made to arrive at the proposed modeling approach, it is instructive to present future improvements to the current formulation while retaining a quasi-steady assumption for analytical tractability. As suggested in a recent review of SOT (Buckley et al., 2016), aerodynamic modifications resulting from the interaction between wind speed and the leaf (represented by boundary-layer conductance; g_b) and the CO₂ transport efficiency in the mesophyll (encoded in the mesophyll conductance; g_m) are required when their magnitudes are comparable with g_s . Regarding g_b , the stomatal behavior can be altered appreciably by g_b even when the state variables such as T_a , CO₂ and water vapor concentrations above the laminar boundary layer remain the same (Huang et al., 2015; Schymanski and Or, 2016). The effects of g_b on g_s have been incorporated into prior models using SOT or profit-maximization (Huang et al., 2015; Sperry et al., 2016a; Wolf et al., 2016). However, g_b was mainly characterized by mean wind speed and effective leaf size using empirical formulations that may not reflect wind contact angle, leaf orientation and the micro-roughness on the leaf surface, and turbulent intensity. With regard to g_m , the effects of g_m on f_c has been considered explicitly in some SOT (Volpe et al., 2011) and compared with empirical data to explore the partitioning between g_s and g_m under salt-stressed conditions when soil water availability is not limited. Evidence that g_m is finite and varies with various environmental factors has been reviewed elsewhere (Flexas et al., 2008), with g_m being reduced during persistent drought conditions (Grassi and Magnani, 2005; Jones, 1973). As suggested elsewhere (Gu and Sun, 2014), however, the dependency of g_m on c_i or irradiance may be artifacts due to measurement methods.

Uncertainties in modeling g_s can be further reduced when the spatio-temporal dynamics of water movement in the soil-xylem hydraulic system are appropriately described. Plant water storage (PWS) and hydraulic redistribution (HR) representing above- and below ground water reservoirs are the two defining features that impact soil-plant hydrodynamics and drought resilience (Domec et al., 2010; Goldstein et al., 1998; Huang et al., 2017; Maherali and DeLucia, 2001; Neumann and Cardon, 2012; Prieto et al., 2012; Stratton et al., 2000). To accommodate the overnight competition for water between PWS and HR in modeling g_s , a multi-layered scheme for solving water mass balance in each soil-plant compartments is required (Huang et al., 2017). The consideration of how the soil-xylem hydraulics (i.e., $K - \psi_l$ relation) is impacted by the delay refilling processes in air-filled xylem conduits (Brodrribb and Cochard, 2009; Sperry and Tyree, 1990) is also required especially when the function of impaired xylem conduits cannot be recovered under water stress condition. When coupled with light attenuation and turbulent flow models, detailed representation of hydraulic architec-

ture (Bohrer et al., 2005; Hentschel et al., 2013; Janott et al., 2011; Manoli et al., 2014; 2017) for individual plant can further assist understanding plant-plant competition for water and light. Despite the plethora of complications to measure or model water relations within the soil-plant system, an exhaustive theoretical treatment for the aforementioned mechanisms may also shed light on how the transport of chemical signals (e.g., abscisic acid) through xylem contributes to stomatal behavior (Tardieu, 2016).

In line with recent studies (Hölttä et al., 2017; Jensen et al., 2016; Lucas et al., 2013; Nikinmaa et al., 2013; Sevanto, 2014; Stroock et al., 2014), the significance of the phloem anatomy and physiology associated with long-distance sucrose transport on g_s cannot be overlooked. At the whole-plant level, sucrose export from the loading phloem here requires further elaboration to account for influences of loading efficiencies with different loading strategies, viscosity built-up due to sucrose accumulation, elastic nature of sieve element, thickness of the sieve plate and distribution of sieve pore radii (Jensen et al., 2012; 2014; Liesche et al., 2015; Thompson and Holbrook, 2003; Turgeon, 2010). How the modifications of osmotic regulation in response to drought stress in each plant compartment impact the transport system (Dichio et al., 2006; Morgan, 1984) should be also accounted for in future modeling efforts. However, the primary challenge remains at the long time-scales. Different from quantifying short time-scales stomatal responses, the difficulty in evaluating how acclimation or adaptation of plant traits respond to the history of environmental conditions can be further accentuated by the fact that the climate system is also sensitive to feedbacks from plants, thereby generating the so-called *feedback cycle*.

4. Conclusion

The significance of biotic controls through stomata on global carbon and water cycles, food production and security, and ecosystem services is rarely disputed. We developed a mathematical model of stomata based on the premise of a coordinated photosynthetic-hydraulic-sucrose transporting machinery. We hypothesize that this coordination evolved to maximize the sucrose mass flux out of the loading leaf. Because we consider that maximizing sucrose mass flux can be readily viewed as maximizing energy flux, we proposed this as a qualitative link to Lodka's maximum energy circulation principle in plants. For a wide range of time-scales, the proposed approach captures the general features of stomatal sensitivity to environmental factors and hydrological states. The proposed framework explains how the carbon and water economies are intrinsically linked by the coordination among the main mass transporting networks within plants that dictates the much debated isohydric-to-anisohydric behavior. To permit analytical foresight, only the main transporting processes impacting g_s are accounted for in the soil-xylem-leaf-phloem system. Variable sucrose sinks and stores from the loading to the unloading zones were not explicitly treated here. Recent research trends are beginning to address carbon allocation and sinks throughout the entire plant system (Fatichi et al., 2014; Hartmann and Trumbore, 2016; Savage et al., 2015) and the framework here must be viewed as one step in this direction. It offers immanent constraints as to how g_s responds to its environment on multiple time-scales pertinent to the xylem-leaf-phloem transport system. Field and laboratory testing of the proposed approach here are topics for future studies.

Acknowledgments

We acknowledge support from the National Science Foundation (NSF-DEB-1557176, NSF-EAR-1344703, NSF-AGS-1644382, NSF-IOS-1754893, and NSF-DGE-1068871), the US Department of Energy (DOE) through the Office of Biological and Environmental Research (BER) Terrestrial Carbon Processes (TCP) program (DE-SC0006967 and DE-SC0011461).

Appendix A. Model derivation

When combining Eqs. (7)–(10), F_E can be expressed as:

$$F_E = Q_c \frac{N_c}{V_p} A_{xp} L_{xp} \left(\psi_l + RT_p \frac{N_c}{V_p} - p_g \right). \quad (\text{A.1})$$

In Eq. (A.1), mechanical pressure (p_p) is assumed to be negligible when compared with osmotic potential ($\Pi = -RT_p N_c / V_p$) over a short period (Jensen et al., 2016). By substituting Eq. (6) into Eq. (A.1), F_E can be now written as a function of ψ_l :

$$F_E(\psi_l) = G [f_c^2(\psi_l) + I(\psi_l - p_g) f_c(\psi_l)], \quad (\text{A.2})$$

where $G = Q_c A_{xp} L_{xp} RT_p (\alpha \beta A_l \Delta t / V_p)^2$ and $I = (V_p / A_l) (\alpha \beta \Delta t RT_p)^{-1}$. When coupling the supply-demand balance of CO_2 (i.e., $f_{c,s} = f_{c,d}$; Eq. (2)) and water (i.e., $f_{e,s} = f_{e,d}$; Eq. (4)) fluxes through g_s , f_c in Eq. (A.2) can be written as a function of ψ_l and directly reflects the limitations imposed by the photosynthetic machinery and soil-xylem hydraulics on F_E (see Section 1).

Now, inserting Eq. (4) (i.e., $\psi_l = \psi_s - (m_v A_l f_e(\psi_l)) / K(\psi_l)$) into Eq. (A.2) to replace ψ_l , Eq. (A.2) can be re-written as:

$$F_E(\psi_l) = G \left[f_c^2(\psi_l) + I \left(\psi_s - \frac{m_v A_l f_e(\psi_l)}{K(\psi_l)} - p_g \right) f_c(\psi_l) \right]. \quad (\text{A.3})$$

Under well-watered soil condition (i.e., $\psi_s \approx 0$) with negligible p_g , the export of energy flux from loading phloem ($F_{E,ww}(\psi_l)$) is subsequently approximated as:

$$F_{E,ww}(\psi_l) = G \left[f_c^2(\psi_l) + m_v I A_l \frac{f_e(\psi_l)}{K(\psi_l)} f_c(\psi_l) \right]. \quad (\text{A.4})$$

Thus, the optimal ψ_l can be obtained by setting $\partial F_{E,ww} / \partial \psi_l = 0$ that yields:

$$\frac{\partial f_c(\psi_l)}{\partial \psi_l} - \frac{m_v I A_l}{2} \left[\underbrace{\frac{f_e(\psi_l)}{K(\psi_l) f_c(\psi_l)} \frac{\partial f_c(\psi_l)}{\partial \psi_l}}_{\text{M}} + \underbrace{\frac{\partial}{\partial \psi_l} \left(\frac{f_e(\psi_l)}{K(\psi_l)} \right)}_{\text{N}} \right] = 0. \quad (\text{A.5})$$

When $\text{M}/\text{N} \ll 1$ (see Appendix B), Eq. (A.5) is reduced to:

$$\frac{\partial f_c(\psi_l)}{\partial \psi_l} - \frac{m_v I A_l}{2} \frac{\partial}{\partial \psi_l} \left(\frac{f_e(\psi_l)}{K(\psi_l)} \right) = 0. \quad (\text{A.6})$$

or

$$\frac{\partial}{\partial \psi_l} \left[f_c(\psi_l) + \frac{I}{2} \psi_l \right] = 0, \quad (\text{A.7})$$

At $\psi_s \approx 0$, the reduction in $K(\psi_l)$ is small and $K(\psi_l)$ can be approximated as K_{\max} (see Appendix B) so that Eq. (A.6) can be further simplified as:

$$\frac{\partial}{\partial \psi_l} \left[f_c(\psi_l) - \frac{m_v I A_l}{2 K_{\max}} f_e(\psi_l) \right] = 0. \quad (\text{A.8})$$

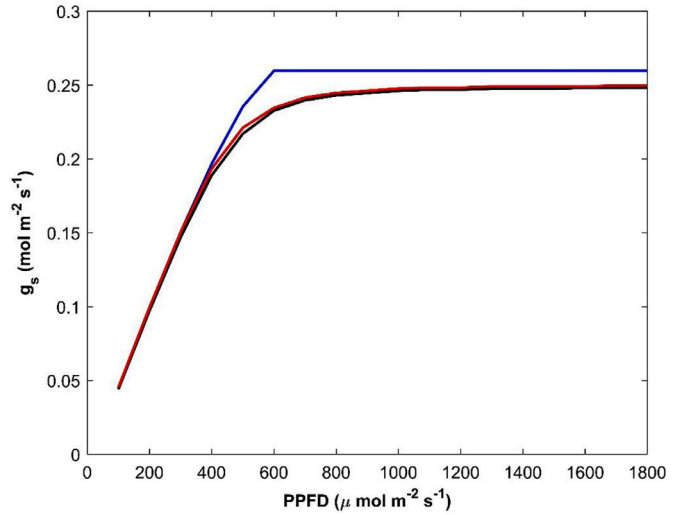


Fig. Appendix B.1. Modeled stomatal conductance (g_s) as a function of photosynthetically active radiation (PPFD) under well-watered condition. The model results calculated from Eqs. (A.2), (A.7) and (A.8) are respectively represented by black, red and blue lines. The physiological, hydraulic and allometric attributes of soil-plant system for coniferous species in general reported elsewhere (Huang et al., 2017) are adopted. Physical characteristics of leaves and anatomical attributes of phloem for *Pinus taeda* L. listed in Table 2 are used. T_w , c_o and RH are respectively fixed to be 25 °C, 400 ppm and 50% while PPFD varies from 100 to 1000 $\text{mol m}^{-2} \text{s}^{-1}$. (For interpretation of the references to color in this figure legend, the reader is referred to the web version of this article.)

Appendix B. Scaling analysis

In Eq. (14), the ratio of M to N can be approximated as:

$$\frac{\text{M}}{\text{N}} = \frac{f_e \frac{\partial f_c}{\partial \psi_l}}{K f_c \frac{\partial}{\partial \psi_l} \left(\frac{f_e}{K} \right)} \approx \frac{f_c}{f_e}^{-1} \frac{\partial f_c}{\partial f_e} \left(1 + \frac{\partial K}{K} \frac{\psi_l}{\partial \psi_l} \right), \quad (\text{B.1})$$

where f_c/f_e is the water use efficiency on the order of 10^{-3} (Huang et al., 2015; Schymanski and Or, 2016), $\partial f_c / \partial f_e$ is the marginal water use efficiency on the order of 10^{-4} – 10^{-3} (Lloyd and Farquhar, 1994; Manzoni et al., 2011), $\partial K / K \approx -10^{-1}$ is the percentage of K loss referenced to maximum K_{\max} at $\psi_s \approx 0$ (i.e., operating $K \approx K_{\max}$) and $\psi_l / \partial \psi_l$ is on the order of 1 because stomatal closure commonly occurs before the air-entry point (i.e., at ψ_l where 12% of K losses occur) (Bond and Kavanagh, 1999; Sparks and Black, 1999), so that $\text{M}/\text{N} \ll 1$.

As shown in Fig. B.1, the difference of modeled g_s between Eqs. (A.8) and (A.2) (or (A.7)) increases with increasing f_e (i.e., a larger PPFD) when soil water status is close to saturation. However, such small difference (i.e., less than 10%) suggests that the approximation of $\text{M}/\text{N} \ll 1$ and the assumption of $K \approx K_{\max}$ adopted in Eq. (A.8) do not significantly impact the model results. If the plant allows that the percentage of K losses can be much larger than 12% (i.e., operating $K \ll K_{\max}$), M in Eq. (A.5) cannot be ignored and Eq. (A.2) is required.

Appendix C. Analytical solution and its approximation of stomatal optimization theory (SOT) under well-watered soil condition

When the supply-demand balance of CO_2 and water fluxes is incorporated into SOT, g_s , c_i and ψ_l can be interchangeable independent variables. For convenience, c_i is selected here as the independent variable and the inverse of $\lambda_X(\Lambda)$ is adopted (Medlyn et al., 2011; Prentice et al., 2014) to derive the analytical solution from SOT, in which the Hamiltonian can be now given as:

$$H_{a,X}(c_i) = f_e(c_i) - \Lambda f_c(c_i). \quad (\text{C.1})$$

Assuming R_d is negligible when compared with f_c , the optimal c_i can be obtained by setting $\partial H_{a,X}(c_i)/\partial c_i = 0$ and is equivalent to the positive root of quadratic function, $Ac_i^2 + Bc_i + C = 0$, where:

$$\begin{aligned} A &= L - (k_2 + \Gamma^*), \\ B &= 2(k_2 + \Gamma^*)c_a - 2L\Gamma^*, \\ C &= -(k_2 + \Gamma^*)c_a^2 + (k_2 + \Gamma^*)Lc_a - k_2\Gamma^*L, \end{aligned} \quad (C.2)$$

where $L = aD/\Lambda$. If $c_i \gg \Gamma^*$ is further assumed, the determinant of quadratic function can be subsequently simplified to (Medlyn et al., 2011):

$$\Delta \approx 4L(k_2 + \Gamma^*)c_a^2. \quad (C.3)$$

Thus, the optimal c_i can be given as:

$$c_i = \frac{-(k_2 + \Gamma^*)c_a + L\Gamma^* + c_a\sqrt{L(k_2 + \Gamma^*)}}{L - (k_2 + \Gamma^*)}. \quad (C.4)$$

Because $c_a > c_i \gg \Gamma^*$, c_i/c_a ratio can be approximated as:

$$\frac{c_i}{c_a} \approx \frac{(k_2 + \Gamma^*) - \sqrt{L(k_2 + \Gamma^*)}}{(k_2 + \Gamma^*) - L}. \quad (C.5)$$

By substituting $L = aD/\Lambda$ and $\Lambda = 1/\lambda_X$ into Eq. (C.5), c_i/c_a ratio and the corresponding $g_{s,ww}$ can be now written as:

$$\begin{aligned} \frac{c_i}{c_a} &= \frac{1}{1 + \sqrt{\frac{aD\lambda_X}{k_2 + \Gamma^*}}} = \frac{\sqrt{\frac{k_2 + \Gamma^*}{a\lambda_X}}}{\sqrt{\frac{k_2 + \Gamma^*}{a\lambda_X}} + \sqrt{D}}, \\ g_{s,ww} &= \left(1 + \sqrt{\frac{k_2 + \Gamma^*}{aD\lambda_X}}\right) \frac{f_c}{c_a}. \end{aligned} \quad (C.6)$$

The c_i/c_a ratio in Eq. (C.6) can be also expressed by Taylor series expansion that is given as:

$$\frac{c_i}{c_a} = \frac{1}{1 + \chi} \approx \Sigma_n (-\chi)^n. \quad (C.7)$$

where $\chi = \sqrt{aD\lambda_X/k_2 + \Gamma^*}$ and $n \in (0, \infty)$ is zero or a positive integer. When χ is relatively small, the higher order terms in Eq. (C.7) can be neglected, leading to the approximation of c_i/c_a ratio and $g_{s,ww}$ that is given as:

$$\begin{aligned} \frac{c_i}{c_a} &= 1 - \sqrt{\frac{a\lambda_X}{k_2 + \Gamma^*}} \sqrt{D}, \\ g_{s,ww} &= \sqrt{\frac{k_2 + \Gamma^*}{a\lambda_X}} \frac{f_c}{c_a} D^{-1/2}. \end{aligned} \quad (C.8)$$

References

Aphalo, P., Jarvis, P., 1991. Do stomata respond to relative humidity? *Plant, Cell Environ.* 14 (1), 127–132.

Baldocchi, D., Meyers, T., 1998. On using eco-physiological, micrometeorological and biogeochemical theory to evaluate carbon dioxide, water vapor and trace gas fluxes over vegetation: a perspective. *Agric. For. Meteorol.* 90 (1), 1–25.

Ball, J.T., Woodrow, I.E., Berry, J.A., 1987. A model predicting stomatal conductance and its contribution to the control of photosynthesis under different environmental conditions. In: *Progress in Photosynthesis Research*. Springer, pp. 221–224.

Ball, M.C., Farquhar, G.D., 1984. Photosynthetic and stomatal responses of two mangrove species, *Aegiceras corniculatum* and *Avicennia marina*, to long term salinity and humidity conditions. *Plant Physiol.* 74 (1), 1–6.

Berner, R.A., 1991. A model for atmospheric CO₂ over phanerozoic time. *Am. J. Sci. (United States)* 291 (4). <https://doi.org/10.2475/ajs.291.4.339>.

Berner, R.A., Kothavalai, Z., 2001. GEOCARB III: a revised model of atmospheric CO₂ over Phanerozoic time. *Am. J. Sci.* 301 (2), 182–204.

Berninger, F., Hari, P., 1993. Optimal regulation of gas exchange: evidence from field data. *Ann. Bot.* 71 (2), 135–140.

Berninger, F., Mäkelä, A., Hari, P., 1996. Optimal control of gas exchange during drought: empirical evidence. *Ann. Bot.* 77 (5), 469–476.

Betts, R., Boucher, O., Collins, M., Cox, P., Falloon, P., Gedney, N., Hemming, D., Huntingford, C., Jones, C., Sexton, D., Webb, M., 2007. Projected increase in continental runoff due to plant responses to increasing carbon dioxide. *Nature* 448 (7157), 1037–1041.

Bohrer, G., Mourad, H., Laursen, T., Drewry, D., Avissar, R., Poggi, D., Oren, R., Katul, G., 2005. Finite element tree crown hydrodynamics model (FETCH) using porous media flow within branching elements: A new representation of tree hydrodynamics. *Water Resour. Res.* 41 (11). <https://doi.org/10.1029/2005WR004181>.

Bond, B.J., Kavanagh, K.L., 1999. Stomatal behavior of four woody species in relation to leaf-specific hydraulic conductance and threshold water potential. *Tree Physiol.* 19 (8), 503–510.

Brodrribb, T., Cochard, H., 2009. Hydraulic failure defines the recovery and point of death in water-stressed conifers. *Plant Physiol.* 149 (1), 575–584.

Buckley, T.N., Sack, L., Farquhar, G.D., 2016. Optimal plant water economy. *Plant, Cell Environ.* <https://doi.org/10.1111/pce.12823>.

Campbell, G.S., Norman, J., 1998. *An Introduction to Environmental Biophysics*. Springer, New York.

Christy, A.L., Ferrier, J.M., 1973. A mathematical treatment of Munch's pressure-flow hypothesis of phloem translocation. *Plant Physiol.* 52 (6), 531–538.

Cowan, I., Farquhar, G., 1977. Stomatal function in relation to leaf metabolism and environment. *Integration of Activity in the Higher Plant. Symposia of the Society for Experimental Biology*, 31. Cambridge University Press, Cambridge.

Cox, P., Betts, R., Jones, C., Spall, S., Totterdell, I., 2000. Acceleration of global warming due to carbon-cycle feedbacks in a coupled climate model. *Nature* 408 (6809), 184–187.

Crombie, D., Hipkins, M., Milburn, J., 1985. Gas penetration of pit membranes in the xylem of *Rhododendron* as the cause of acoustically detectable sap cavitation. *Funct. Plant Biol.* 12 (5), 445–453.

Damour, G., Simonneau, T., Cochard, H., Urban, L., 2010. An overview of models of stomatal conductance at the leaf level. *Plant, Cell Environ.* 33 (9), 1419–1438.

Dannoura, M., Maillard, P., Fresneau, C., Plain, C., Berveiller, D., Gerant, D., Chipeaux, C., Bosc, A., Ngao, J., Damesin, C., 2011. In situ assessment of the velocity of carbon transfer by tracing ¹³C in trunk CO₂ efflux after pulse labelling: variations among tree species and seasons. *New Phytol.* 190 (1), 181–192.

Dichio, B., Xiloyannis, C., Sofo, A., Montanaro, G., 2006. Osmotic regulation in leaves and roots of olive trees during a water deficit and rewetting. *Tree Physiol.* 26 (2), 179–185.

Dixon, H.H., Joly, J., 1895. On the ascent of sap. *Philos. Trans. R. Soc. London. B* 186, 563–576.

Domec, J., Gartner, B., 2001. Cavitation and water storage capacity in bole xylem segments of mature and young Douglas-fir trees. *Trees* 15 (4), 204–214.

Domec, J., King, J.S., Noormets, A., Treasure, E., Gavazzi, M., Sun, G., McNulty, S., 2010. Hydraulic redistribution of soil water by roots affects wholestand evapotranspiration and net ecosystem carbon exchange. *New Phytol.* 187 (1), 171–183.

Domec, J., Palmroth, S., Ward, E., Maier, C.A., Thérizien, M., Oren, R., 2009. Acclimation of leaf hydraulic conductance and stomatal conductance of *Pinus taeda* (loblolly pine) to long-term growth in elevated CO₂ (free-air CO₂ enrichment) and N-fertilization. *Plant, Cell Environ.* 32 (11), 1500–1512.

Domec, J., Smith, D.D., McCulloh, K.A., 2016. A synthesis of the effects of atmospheric carbon dioxide enrichment on plant hydraulics: implications for whole-plant water use efficiency and resistance to drought. *Plant, Cell Environ.* <https://doi.org/10.1111/pce.12843>.

Domec, J.-C., Johnson, D.M., 2012. Does homeostasis or disturbance of homeostasis in minimum leaf water potential explain the isohydric versus anisohydric behavior of *Vitis vinifera* L. cultivars? *Tree Physiol.* 32 (3), 245–248.

Domec, J.-C., Palmroth, S., Oren, R., 2016. Effects of *Pinus taeda* leaf anatomy on vascular and extravascular leaf hydraulic conductance as influenced by N-fertilization and elevated CO₂. *J. Plant Hydraul.* 3, 007.

Drake, B.G., González-Meler, M.A., Long, S.P., 1997. More efficient plants: A consequence of rising atmospheric CO₂? *Annu. Rev. Plant Biol.* 48 (1), 609–639.

Ehleringer, J.R., Cerling, T.E., 1995. Atmospheric CO₂ and the ratio of intercellular to ambient CO₂ concentrations in plants. *Tree Physiol.* 15 (2), 105–111.

Ellsworth, D.S., Thomas, R., Crous, K.Y., Palmroth, S., Ward, E., Maier, C., DeLucia, E., Oren, R., 2012. Elevated CO₂ affects photosynthetic responses in canopy pine and subcanopy deciduous trees over 10 years: a synthesis from Duke Face. *Glob. Chang. Biol.* 18 (1), 223–242.

Farquhar, G., Schulze, E., Koppers, M., 1980. Responses to humidity by stomata of *Nicotiana glauca* L. and *Corylus avellana* L. are consistent with the optimization of carbon dioxide uptake with respect to water loss. *Funct. Plant Biol.* 7 (3), 315–327.

Farquhar, G.D., von Caemmerer, S., Berry, J.A., 1980. A biochemical model of photosynthetic CO₂ assimilation in leaves of C₃ species. *Planta* 149 (1), 78–90.

Faticchi, S., Leuzinger, S., Koerner, C., 2014. Moving beyond photosynthesis: from carbon source to sinkdriven vegetation modeling. *New Phytol.* 201 (4), 1086–1095.

Flexas, J., Ribas-Carbo, M., Diaz-Ortega, A., Galmés, J., Medrano, H., 2008. Mesophyll conductance to CO₂: current knowledge and future prospects. *Plant, Cell Environ.* 31 (5), 602–621.

Gedney, N., Cox, P., Betts, R., Boucher, O., Huntingford, C., Stott, P., 2006. Detection of a direct carbon dioxide effect in continental river runoff records. *Nature* 439 (7078), 835–838.

Givnish, T.J., Vermeij, G.J., 1976. Sizes and shapes of liane leaves. *Am. Nat.* 110 (975), 743–778.

Goldstein, G., Andrade, J., Meinzer, F., Holbrook, N., Cavelier, J., Jackson, P., Celis, A., 1998. Stem water storage and diurnal patterns of water use in tropical forest canopy trees. *Plant, Cell Environ.* 21 (4), 397–406.

Grantz, D., 1990. Plant response to atmospheric humidity. *Plant, Cell Environ.* 13 (7), 667–679.

Grassi, G., Magnani, F., 2005. Stomatal, mesophyll conductance and biochemical limitations to photosynthesis as affected by drought and leaf ontogeny in ash and oak trees. *Plant, Cell Environ.* 28 (7), 834–849.

Gratani, L., 2014. Plant phenotypic plasticity in response to environmental factors. *Adv. Botany* 2014.

Gu, L., Sun, Y., 2014. Artefactual responses of mesophyll conductance to CO_2 and irradiance estimated with the variable J and online isotope discrimination methods. *Plant, Cell Environ.* 37 (5), 1231–1249.

Hari, P., Mäkelä, A., Korpilahti, E., Holmberg, M., 1986. Optimal control of gas exchange. *Tree Physiol.* 2 (1–2–3), 169–175.

Hartmann, H., Trumbore, S., 2016. Understanding the roles of nonstructural carbohydrates in forest trees from what we can measure to what we want to know. *New Phytol.* 211 (2), 386–403.

Hentschel, R., Bittner, S., Janott, M., Biernath, C., Holst, J., Ferrio, J.P., Gessler, A., Priesack, E., 2013. Simulation of stand transpiration based on a xylem water flow model for individual trees. *Agric. For. Meteorol.* 182, 31–42.

Hetherington, A.M., Woodward, F.I., 2003. The role of stomata in sensing and driving environmental change. *Nature* 424 (6951), 901–908.

Hölttä, T., Lintunen, A., Chan, T., Mäkelä, A., Nikinmaa, E., 2017. A steady-state stomatal model of balanced leaf gas exchange, hydraulics and maximal source-sink flux. *Tree Physiol.* 1–18.

Hölttä, T., Vesala, T., Sevanto, S., Perämäki, M., Nikinmaa, E., 2006. Modeling xylem and phloem water flows in trees according to cohesion theory and Münch hypothesis. *Trees* 20 (1), 67–78.

Huang, C.-W., Chu, C.-R., Hsieh, C.-I., Palmroth, S., Katul, G.G., 2015. Wind-induced leaf transpiration. *Adv. Water Resour.* 86, 240–255. <https://doi.org/10.1016/j.advwatres.2015.10.009>.

Huang, C.-W., Domec, J.-C., Ward, E.J., Duman, T., Manoli, G., Parolari, A.J., Katul, G.G., 2017. The effect of plant water storage on water fluxes within the coupled soil-plant system. *New Phytol.* 213 (3), 1093–1106. <https://doi.org/10.1111/nph.14273>.

Janott, M., Gayler, S., Gessler, A., Javaux, M., Klier, C., Priesack, E., 2011. A one-dimensional model of water flow in soil-plant systems based on plant architecture. *Plant Soil* 341 (1), 233–256.

Jensen, K.H., Berg-Srensen, K., Bruus, H., Holbrook, N.M., Liesche, J., Schulz, A., Zwieniecki, M.A., Bohr, T., 2016. Sap flow and sugar transport in plants. *Rev. Mod. Phys.* 88 (3), 035007.

Jensen, K.H., Lee, J., Bohr, T., Bruus, H., Holbrook, N., Zwieniecki, M., 2011. Optimality of the Münch mechanism for translocation of sugars in plants. *J. R. Soc. Interface* 8 (61), 1155–1165.

Jensen, K.H., Mullendore, D.L., Holbrook, N.M., Bohr, T., Knoblauch, M., Bruus, H., 2012. Modeling the hydrodynamics of phloem sieve plates. *Front. Plant Sci.* 3 (151).

Jensen, K.H., Valente, A.X., Stone, H.A., 2014. Flow rate through microfilters: Influence of the pore size distribution, hydrodynamic interactions, wall slip, and inertia. *Phys. Fluids* 26 (5), 052004.

Jones, H.G., 1973. Moderate-term water stresses and associated changes in some photosynthetic parameters in cotton. *New Phytol.* 72 (5), 1095–1105.

Juang, J., Katul, G.G., Siqueira, M., Stoy, P., McCarthy, H., 2008. Investigating a hierarchy of eulerian closure models for scalar transfer inside forested canopies. *Boundary Layer Meteorol.* 128 (1), 1–32.

Katul, G.G., Manzoni, S., Palmroth, S., Oren, R., 2010. A stomatal optimization theory to describe the effects of atmospheric CO_2 on leaf photosynthesis and transpiration. *Ann. Bot.* 105 (3), 431–442.

Katul, G.G., Oren, R., Manzoni, S., Higgins, C., Parlange, M.B., 2012. Evapotranspiration: A process driving mass transport and energy exchange in the soil-plant-atmosphere-climate system. *Rev. Geophys.* 50 (3), RG3002. <https://doi.org/10.1029/2011RG000366>.

Katul, G.G., Palmroth, S., Oren, R., 2009. Leaf stomatal responses to vapour pressure deficit under current and CO_2 -enriched atmosphere explained by the economics of gas exchange. *Plant, Cell Environ.* 32 (8), 968–979.

Klein, T., 2014. The variability of stomatal sensitivity to leaf water potential across tree species indicates a continuum between isohydric and anisohydric behaviours. *Funct. Ecol.* 28 (6), 1313–1320.

Kolb, K., Sperry, J.S., 1999. Transport constraints on water use by the great basin shrub, *artemisia tridentata*. *Plant Cell Environ.* 22 (8), 925–936.

Konrad, W., Roth-Nebelsick, A., Grein, M., 2008. Modelling of stomatal density response to atmospheric CO_2 . *J. Theor. Biol.* 253 (4), 638–658.

Lai, C., Katul, G., Oren, R., Ellsworth, D., Schäfer, K., 2000. Modeling CO_2 and water vapor turbulent flux distributions within a forest canopy. *J. Geophys. Res.* 105 (D21), 26333–26351.

Lange, O.L., Lösch, R., Schulze, E., Kappen, L., 1971. Responses of stomata to changes in humidity. *Planta* 100 (1), 76–86.

Lendzion, J., Leuschner, C., 2008. Growth of european beech (*Fagus sylvatica*) saplings is limited by elevated atmospheric vapour pressure deficits. *For. Ecol. Manage.* 256 (4), 648–655.

Leuning, R., 1995. A critical appraisal of a combined stomatal-photosynthesis model for C_3 plants. *Plant, Cell Environ.* 18 (4), 339–355.

Liesche, J., Windt, C., Bohr, T., Schulz, A., Jensen, K.H., 2015. Slower phloem transport in gymnosperm trees can be attributed to higher sieve element resistance. *Tree Physiol.* 35, 376–386.

Lloyd, J., Farquhar, G.D., 1994. ^{13}C discrimination during CO_2 assimilation by the terrestrial biosphere. *Oecologia* 99 (3/4), 201–215.

Lotka, A.J., 1922. Contribution to the energetics of evolution. *Proc. Natl. Acad. Sci. U.S.A.* 8 (6), 147.

Lucas, W.J., Groover, A., Lichtenberger, R., Furuta, K., Yadav, S., Helariutta, Y., He, X., Fukuda, H., Kang, J., Brady, S.M., 2013. The plant vascular system: evolution, development and functions. *J. Integr. Plant Biol.* 55 (4), 294–388.

Maherali, H., DeLucia, E., 2001. Influence of climate-driven shifts in biomass allocation on water transport and storage in ponderosa pine. *Oecologia* 129 (4), 481–491.

Manoli, G., Bonetti, S., Domec, J.-C., Putti, M., Katul, G., Marani, M., 2014. Tree root systems competing for soil moisture in a 3D soil-plant model. *Adv. Water Resour.* 66, 32–42.

Manoli, G., Huang, C.-W., Bonetti, S., Domec, J.-C., Marani, M., Katul, G., 2017. Competition for light and water in a coupled soil-plant system. *Adv. Water Resour.* 108, 216–230.

Mansfield, T., Hetherington, A., Atkinson, C., 1990. Some current aspects of stomatal physiology. *Annu. Rev. Plant Biol.* 41 (1), 55–75.

Manzoni, S., Katul, G., Porporato, A., 2014. A dynamical system perspective on plant hydraulic failure. *Water Resour. Res.* 50 (6), 5170–5183.

Manzoni, S., Vico, G., Katul, G., Fay, P.A., Polley, W., Palmroth, S., Porporato, A., 2011. Optimizing stomatal conductance for maximum carbon gain under water stress: a meta-analysis across plant functional types and climates. *Funct. Ecol.* 25 (3), 456–467.

Manzoni, S., Vico, G., Katul, G., Palmroth, S., Jackson, R.B., Porporato, A., 2013. Hydraulic limits on maximum plant transpiration and the emergence of the safety-efficiency trade-off. *New Phytol.* 198 (1), 169–178.

Manzoni, S., Vico, G., Palmroth, S., Porporato, A., Katul, G., 2013. Optimization of stomatal conductance for maximum carbon gain under dynamic soil moisture. *Adv. Water Resour.* 62, 90–105.

Martínez-Vilalta, J., García-Forner, N., 2017. Water potential regulation, stomatal behaviour and hydraulic transport under drought: deconstructing the iso/anisohydric concept. *Plant, Cell Environ.* 40 (6), 962–976.

Massman, W., Kaufmann, M., 1991. Stomatal response to certain environmental factors: a comparison of models for subalpine trees in the rocky mountains. *Agric. For. Meteorol.* 54 (2–4), 155–167.

McAdam, S.A., Brodrribb, T.J., 2015. The evolution of mechanisms driving the stomatal response to vapor pressure deficit. *Plant Physiol.* 167 (3), 833–843.

McCarthy, H.R., Oren, R., Finzi, A.C., Ellsworth, D.S., KIM, H., Johnsen, K.H., Millar, B., 2007. Temporal dynamics and spatial variability in the enhancement of canopy leaf area under elevated atmospheric CO_2 . *Glob. Chang. Biol.* 13 (12), 2479–2497.

McDowell, N., Pockman, W.T., Allen, C.D., Breshears, D.D., Cobb, N., Kolb, T., Plaut, J., Sperry, J., West, A., Williams, D.G., 2008. Mechanisms of plant survival and mortality during drought: why do some plants survive while others succumb to drought? *New Phytol.* 178 (4), 719–739.

Medlyn, B.E., Duursma, R.A., Eamus, D., Ellsworth, D.S., Prentice, I.C., Barton, C.V., Crous, K.Y., de Angelis, P., Freeman, M., Wingate, L., 2011. Reconciling the optimal and empirical approaches to modelling stomatal conductance. *Glob. Chang. Biol.* 17 (6), 2134–2144.

Meinzer, F.C., Woodruff, D.R., Marias, D.E., Smith, D.D., McCulloh, K.A., Howard, A.R., Magedman, A.L., 2016. Mapping hydroscapes along the iso- to anisohydric continuum of stomatal regulation of plant water status. *Ecol. Lett.* 19 (11), 1343–1352. <https://doi.org/10.1111/ele.12670>.

Mencuccini, M., Hölttä, T., 2010. The significance of phloem transport for the speed with which canopy photosynthesis and belowground respiration are linked. *New Phytol.* 185 (1), 189–203.

Messinger, S.M., Buckley, T.N., Mott, K.A., 2006. Evidence for involvement of photosynthetic processes in the stomatal response to CO_2 . *Plant Physiol.* 140 (2), 771–778.

Monteith, J., 1995. A reinterpretation of stomatal responses to humidity. *Plant, Cell Environ.* 18 (4), 357–364.

Morgan, J.M., 1984. Osmoregulation and water stress in higher plants. *Annu. Rev. Plant Physiol.* 35 (1), 299–319.

Morison, J.I., 1998. Stomatal response to increased CO_2 concentration. *J. Exp. Bot.* 49 (Special Issue), 443–452.

Morison, J.I., Gifford, R.M., 1983. Stomatal sensitivity to carbon dioxide and humidity. A comparison of two C_3 and two C_4 grass species. *Plant Physiol.* 71 (4), 789–796.

Mott, K.A., 1988. Do stomata respond to CO_2 concentrations other than intercellular? *Plant Physiol.* 86 (1), 200–203.

Mullendore, D.L., Windt, C.W., Van As, H., Knoblauch, M., 2010. Sieve tube geometry in relation to phloem flow. *Plant Cell* 22 (3), 579–593.

Neumann, R., Cardon, Z., 2012. The magnitude of hydraulic redistribution by plant roots: a review and synthesis of empirical and modeling studies. *New Phytol.* 194 (2), 337–352.

Nikinmaa, E., Hölttä, T., Hari, P., Kolari, P., Mäkelä, A., Sevanto, S., Vesala, T., 2013. Assimilate transport in phloem sets conditions for leaf gas exchange. *Plant, Cell Environ.* 36 (3), 655–669.

Nobel, P.S., 2009. *Physicochemical and Environmental Plant Physiology*. Academic press, Boston.

Novick, K.A., Minit, C.F., Vose, J.M., 2016. Drought limitations to leaf level gas exchange: results from a model linking stomatal optimization and cohesion tension theory. *Plant, Cell Environ.* 39 (3), 583–596. <https://doi.org/10.1111/pce.12657>.

Odum, H.T., Hall, C.A., 1995. *Maximum Power: The Ideas and Applications of HT Odum*. University Press of Colorado.

Oren, R., Sperry, J.S., Katul, G., Pataki, D.E., Ewers, B., Phillips, N., Schäfer, K., 1999. Survey and synthesis of intra- and interspecific variation in stomatal sensitivity to vapour pressure deficit. *Plant, Cell Environ.* 22 (12), 1515–1526.

Paschalidis, A., Katul, G.G., Fatici, S., Palmroth, S., Way, D., 2017. On the variability of the ecosystem response to elevated atmospheric CO_2 across spatial and temporal scales at the duke forest FACE experiment. *Agric. For. Meteorol.* 232, 367–383.

Pittermann, J., 2010. The evolution of water transport in plants: an integrated approach. *Geobiology* 8 (2), 112–139.

Prentice, I.C., Dong, N., Gleason, S.M., Maire, V., Wright, I.J., 2014. Balancing the costs of carbon gain and water transport: testing a new theoretical framework for plant functional ecology. *Ecol. Lett.* 17 (1), 82–91.

Prieto, I., Armas, C., Pugnaire, F., 2012. Water release through plant roots: new insights into its consequences at the plant and ecosystem level. *New Phytol.* 193 (4), 830–841.

Savage, J.A., Clearwater, M.J., Haines, D.F., Klein, T., Mencuccini, M., Sevanto, S., Turgeon, R., Zhang, C., 2015. Allocation, stress tolerance and carbon transport in

plants: how does phloem physiology affect plant ecology? *Plant, Cell Environ.* 39 (4), 709–725.

Schultz, H.R., 2003. Differences in hydraulic architecture account for nearisohydric and anisohydric behaviour of two fieldgrown *Vitis vinifera* L. cultivars during drought. *Plant, Cell Environ.* 26 (8), 1393–1405.

Schulze, E.-D., Lange, O., Evenari, M., Kappen, L., Buschbom, U., 1974. The role of air humidity and leaf temperature in controlling stomatal resistance of *Prunus armeniaca* L. under desert conditions. *Oecologia* 17 (2), 159–170.

Schymanski, S.J., Or, D., 2016. Wind increases leaf water use efficiency. *Plant, Cell Environ.* 39 (7), 1448–1459.

Sellers, P., Bounoua, L., Collatz, G., Randall, D., Dazlich, D., Los, S., Berry, J., Fung, I., Tucker, C., Field, C., Jensen, T., 1996. Comparison of radiative and physiological effects of doubled atmospheric CO_2 on climate. *Science* 271 (5254), 1402–1406.

Sellers, P., Meeson, B., Hall, F., Asrar, G., Murphy, R., Schiffer, R., Bretherton, F., Dickinson, R., Ellingson, R., Field, C., Huemmrich, K., Justice, C., Melack, J., Roulet, N., Schimel, D., Try, P., 1995. Remote sensing of the land surface for studies of global change: Models-algorithms-experiments. *Remote Sens. Environ.* 51 (1), 3–26.

Sevanto, S., 2014. Phloem transport and drought. *J. Exp. Bot.* 65 (7), 1751. <https://doi.org/10.1093/jxb/ert467>.

Sevanto, S., McDowell, N.G., Dickman, L.T., Pangle, R., Pockman, W.T., 2014. How do trees die? a test of the hydraulic failure and carbon starvation hypotheses. *Plant, Cell Environ.* 37 (1), 153–161.

Siqueira, M., Katul, G., 2002. Estimating heat sources and fluxes in thermally stratified canopy flows using higher-order closure models. *Boundary Layer Meteorol.* 103 (1), 125–142.

Sparkes, J., Black, R., 1999. Regulation of water loss in populations of *Populus trichocarpa*: the role of stomatal control in preventing xylem cavitation. *Tree Physiol.* 19 (7), 453–459.

Sperry, J., Adler, F., Campbell, G., Comstock, J., 1998. Limitation of plant water use by rhizosphere and xylem conductance: results from a model. *Plant, Cell Environ.* 21 (4), 347–359.

Sperry, J., Hacke, U., Oren, R., Comstock, J., 2002. Water deficits and hydraulic limits to leaf water supply. *Plant, Cell Environ.* 25 (2), 251–263.

Sperry, J., Love, D., 2015. What plant hydraulics can tell us about responses to climate-change droughts. *New Phytol.* 207, 14–27.

Sperry, J., Tyree, M., 1988. Mechanism of water stress-induced xylem embolism. *Plant Physiol.* 88 (3), 581–587.

Sperry, J., Tyree, M., 1990. Water-stress-induced xylem embolism in three species of conifers. *Plant, Cell Environ.* 13 (5), 427–436.

Sperry, J.S., 2003. Evolution of water transport and xylem structure. *Int. J. Plant Sci.* 164 (S3), S115–S127.

Sperry, J.S., Venturas, M.D., Anderegg, W.R., Mencuccini, M., Mackay, D.S., Wang, Y., Love, D.M., 2016. Predicting stomatal responses to the environment from the optimization of photosynthetic gain and hydraulic cost. *Plant, Cell Environ.* <https://doi.org/10.1111/pce.12852>.

Sperry, J.S., Wang, Y., Wolfe, B.T., Mackay, D.S., Anderegg, W.R., McDowell, N.G., Pockman, W.T., 2016. Pragmatic hydraulic theory predicts stomatal responses to climatic water deficits. *New Phytol.* 212 (3), 577–589.

Stratton, L., Goldstein, G., Meinzer, F., 2000. Stem water storage capacity and efficiency of water transport: their functional significance in a hawaiian dry forest. *Plant, Cell Environ.* 23 (1), 99–106.

Stroock, A.D., Pagay, V.V., Zwieniecki, M.A., Michele Holbrook, N., 2014. The physico-chemical hydrodynamics of vascular plants. *Annu. Rev. Fluid Mech.* 46, 615–642.

Tardieu, F., 2016. Too many partners in rootshoot signals. does hydraulics qualify as the only signal that feeds back over time for reliable stomatal control? *New Phytol.* 212 (4), 802–804.

Thompson, M., Holbrook, N.M., 2003. Application of a single-solute non-steady-state phloem model to the study of long-distance assimilate transport. *J. Theor. Biol.* 220 (4), 419–455.

Thompson, S.E., Katul, G.G., 2012. Hydraulic determinism as a constraint on the evolution of organisms and ecosystems. *J. Hydraul. Res.* 50 (6), 547–557.

Tor-ngern, P., Oren, R., Ward, E.J., Palmroth, S., McCarthy, H.R., Domec, J., 2015. Increases in atmospheric CO_2 have little influence on transpiration of a temperate forest canopy. *New Phytol.* 205 (2), 518–525.

Turgeon, R., 2010. The role of phloem loading reconsidered. *Plant Physiol.* 152 (4), 1817–1823.

Tuzet, A., Perrier, A., Leuning, R., 2003. A coupled model of stomatal conductance, photosynthesis and transpiration. *Plant, Cell Environ.* 26 (7), 1097–1116.

Vico, G., Manzoni, S., Palmroth, S., Weih, M., Katul, G., 2013. A perspective on optimal leaf stomatal conductance under CO_2 and light co-limitations. *Agric. For. Meteorol.* 182, 191–199.

Volpe, V., Manzoni, S., Marani, M., Katul, G., 2011. Leaf conductance and carbon gain under salt-stressed conditions. *J. Geophys. Res.-Biogeosci.* 116 (G4), G04035. <https://doi.org/10.1029/2011JG001848>.

Windt, C.W., Vergeldt, F.J., De Jager, P.A., Van As, H., 2006. MRI Of longdistance water transport: a comparison of the phloem and xylem flow characteristics and dynamics in poplar, castor bean, tomato and tobacco. *Plant, Cell Environ.* 29 (9), 1715–1729.

Wolf, A., Anderegg, W.R., Pacala, S.W., 2016. Optimal stomatal behavior with competition for water and risk of hydraulic impairment. *Proc. Natl. Acad. Sci.* 113 (46), E7222–E7230.

Wong, S., Cowan, I., Farquhar, G., 1979. Stomatal conductance correlates with photosynthetic capacity. *Nature* 282 (5737), 424–426.